Geosci. Model Dev. Discuss., doi:10.5194/gmd-2016-14, 2016
Manuscript under review for journal Geosci. Model Dev.
Published: 10 May 2016


Geoscientific Model Development Discussions
Open Access
EGU

# The carbon cycle in the Australian Community Climate and Earth System Simulator (ACCESS-ESM1). 2. Historical simulations

Tilo Ziehn[1], Andrew Lenton[2], Rachel M. Law[1], Richard J. Matear[2], and Matthew A. Chamberlain[2]

[1]CSIRO Oceans and Atmosphere, PMB 1, Aspendale, Victoria, Australia
[2]CSIRO Oceans and Atmosphere, Hobart, Tasmania, Australia

*Correspondence to:* Tilo Ziehn (tilo.ziehn@csiro.au)

**Abstract.** Over the last decade many climate models have evolved into earth system models (ESMs), which are able to simulate both physical and biogeochemical processes through the inclusion of additional components such as the carbon cycle. The Australian Community Climate and Earth System Simulator (ACCESS) has been recently extended to include land and ocean carbon cycle components in its ACCESS-ESM1 version. A detailed description of ACCESS-ESM1 components including results from pre-industrial simulations is provided in Part 1. Here, we focus on the evaluation of ACCESS-ESM1 over the historical period (1850-2005) in terms of its capability to reproduce climate and carbon related variables. Comparisons are performed with observations, if available, but also with other ESMs to highlight common weaknesses. We find that climate variables controlling the exchange of carbon are well reproduced, however ACCESS-ESM1 is somewhat over-sensitive to anthropogenic aerosols which leads to an overly strong cooling response in the land from about 1960 onwards. The land carbon cycle is evaluated for two scenarios: running with a prescribed leaf area index (LAI) and running with a prognostic LAI. We overestimate the seasonal amplitude of the prognostic LAI at the global scale, which is common amongst CMIP5 ESMs. However, the prognostic LAI is our preferred choice, because it allows for the vegetation feedback through the coupling between LAI and the leaf carbon pool. Globally integrated land-atmosphere and ocean-atmosphere fluxes and flux patterns are well reproduced and show good agreement with most recent observations. The seasonal cycle of simulated atmospheric $CO_2$ is close to the observed seasonal cycle, but shows a larger amplitude in the high northern latitudes. Overall, ACCESS-ESM1 performs well over the historical period, making it a useful tool to explore the change in land and oceanic carbon uptake in the future.

## 1 Introduction

Climate models are continuously evolving to include more processes and interactions at higher resolutions and their number has increased rapidly in recent years. In addition, a number of institutes worldwide have been developing earth system models (ESMs), which are able to simulate both physical and biogeochemical processes, through the inclusion of the land and ocean carbon cycles.

Geosci. Model Dev. Discuss., doi:10.5194/gmd-2016-14, 2016
Manuscript under review for journal Geosci. Model Dev.
Published: 10 May 2016


Geoscientific Model Development Discussions
Open Access
EGU

The evaluation of ESMs in terms of their capability to reproduce climate and carbon related variables over the historical period (i.e. 1850 to 2005) is crucial prior to using such models for future predictions. Comparisons are usually performed with observation based products, if available, but also with other ESMs to identify common weaknesses.

The performance of 18 ESMs that participated in the Coupled Model Intercomparison Project phase 5 (CMIP5) (Taylor et al., 2012) has been evaluated in Anav et al. (2013) for the present day climate. They found that all models correctly reproduce the main climate variables controlling the spatial and temporal variability of the carbon cycle. However, large differences exist when reproducing specific fields. In terms of the land carbon cycle an overestimation of photosynthesis and leaf area index (LAI) was found for most of the models. In contrast, for the ocean an underestimation of the primary production was noted for a number of models. Anav et al. (2013) also found significant regional variations in model performance.

Eight of these CMIP5 ESMs were also evaluated in Shao et al. (2013), highlighting that temporal correlations between annual-mean carbon cycle and climate variables vary substantially among the 8 models. Large inter-model disagreements were found for net primary production (NPP) and heterotrophic respiration (Rh). In agreement with Anav et al. (2013), Shao et al. (2013) also noted that the CMIP5 historical simulations tend to overestimate photosynthesis and LAI.

Todd-Brown et al. (2013) compared and evaluated 11 CMIP5 ESMs in terms of their variations in soil carbon. The correct representation of soil carbon in the model is important in order to accurately predict future climate-carbon feedbacks. Soil carbon simulations of the 11 models were compared against empirical data from the Harmonized World Soil Database (HWSD) and from the Northern Circumpolar Soil Carbon Database (NCSCD). A large spread across all models was found (nearly 6 fold) and the spatial distribution of soil carbon especially in the northern latitudes was found to be poor in comparison to HWSD and NCSCD, which means that most ESMs were poorly representing grid-scale soil carbon.

Frölicher et al. (2015) showed that CMIP5 models appeared to capture the observed pattern of anthropogenic carbon storage in the ocean, particularly in the Southern Ocean. However overall they underestimate the magnitude of the observed oceanic global anthropogenic carbon storage since the pre-industrial.

The representation of the global carbon cycle in ESMs continues to be challenging. For example, large uncertainties exist for the climate-carbon feedback, which can be mainly attributed to terrestrial carbon cycle components (Friedlingstein et al., 2006; Arora et al., 2013). Terrestrial ecosystem models show large variations when driven with future climate scenarios (Shao et al., 2013; Friend et al., 2014) due to differences in model formulation and uncertainties in process parameters (Knorr and Heimann, 2001; Booth et al., 2012).

The Australian Community Climate and Earth System Simulator participated in CMIP5 but in a climate model only version. A selection of CMIP5 simulations have now been performed with the ESM version of ACCESS, ACCESS-ESM1 (Law et al., 2015). Here, we present the performance of the land and ocean carbon cycle components of ACCESS-ESM1 over the historical period (1850-2005). First we briefly assess ACCESS-ESM1 simulation of climate variables that are relevant to the carbon cycle (Sect. 3). We then focus on the response of the carbon cycle to the historical forcing (Sect. 4) and comparison of various present-day simulated carbon variables with observations (Sect. 5). Law et al. (2015) provides complementary analysis of the ACCESS-ESM1 pre-industrial simulation.

Geosci. Model Dev. Discuss., doi:10.5194/gmd-2016-14, 2016
Manuscript under review for journal Geosci. Model Dev.
Published: 10 May 2016




## 2 Model configuration, simulations and comparison data

Historical simulations (Sect. 2.2) are performed with two model configurations (Sect. 2.1) and the results compared with other CMIP5 ESMs (Sect. 2.3) and a number of observed data products (Sect. 2.4).

### 2.1 Model configuration

ACCESS-ESM1 is based on the ACCESS climate model (Bi et al., 2013), but with the addition of biogeochemical components for ocean and land as described in part 1 of this paper (Law et al., 2015). The climate model version underlying the ESM version is ACCESS1.4, a minor update of the ACCESS1.3 version submitted to CMIP5 (Bi et al., 2013; Dix et al., 2013). The relationship between the ACCESS1.3, ACCESS1.4 and ACCESS-ESM1 versions is illustrated in Law et al. (2015, Fig. 1). Law et al. (2015) also showed that the climate simulations of the three model versions are very similar.

For the ACCESS-ESM1 version, ocean carbon fluxes are simulated by the World Ocean Model of Biogeochemistry And Trophic dynamics (WOMBAT) (Oke et al., 2013) and land carbon fluxes are simulated by the Community Atmosphere Biosphere Land Exchange (CABLE) model (Kowalczyk et al., 2006; Wang et al., 2011) which optionally includes nutrient limitation (nitrogen and phosphorus) for the terrestrial biosphere through its biogeochemical module, denoted CASA-CNP (Wang et al., 2010). This capability is important because nitrogen, phosphorus and carbon biogeochemical cycles are strongly coupled and it has been demonstrated that nutrient limitation has a large impact on the productivity of terrestrial ecosystems (Wang et al., 2010; Goll et al., 2012; Zhang et al., 2013). Consequently global land carbon uptake can be altered significantly. Here we run CASA-CNP in 'CNP' mode with both nitrogen and phosphorus limitation active. This differentiates the ACCESS-ESM1 simulations presented here from other ESM simulations for CMIP5, few of which included nitrogen and none of which included phosphorus.

As in Law et al. (2015), two model configurations are used, differing in their treatment of leaf area index (LAI). LAI is an important variable in climate models for describing the biophysical and biogeochemical properties of the land cover and in CABLE it can either be prescribed or simulated. When prescribed, monthly values based on MODIS observations are read in through an external file (Law et al., 2015, Sec. 3.1.1). The dataset used here is limited by having no interannual or longer time-scale variability. Additionally the same LAI is assigned to all plant funtional types (PFTs) within a grid-cell even though CABLE simulates multiple PFTs per grid-cell. With prescribed LAI there is no coupling between the LAI and the leaf carbon pool which means that vegetation feedbacks cannot be included. These limitations are removed by making LAI a prognostic variable with the LAI dependent on the simulated size of the leaf carbon pool. However if the leaf carbon pool is not well simulated then this would lead to a poor LAI simulation with consequent impacts for the climate simulation.

### 2.2 Simulations

All experiments are set up as concentration driven simulations, which means that (historical) atmospheric $CO_2$ concentrations are prescribed as an input to ACCESS-ESM1 and changes in the land and ocean carbon pools do not feed back on to atmospheric $CO_2$ concentrations following CMIP5 protocols (Taylor et al., 2012).

Geosci. Model Dev. Discuss., doi:10.5194/gmd-2016-14, 2016
Manuscript under review for journal Geosci. Model Dev.
Published: 10 May 2016


Geoscientific Model Development Discussions

As noted above we run ACCESS-ESM1 in two configurations, with prescribed LAI (PresLAI) and prognostic LAI (ProgLAI). For PresLAI, the carbon cycle has no impact on the simulated climate whereas for ProgLAI, there is a small impact on the climate through biogeophysical feedbacks related to surface albedo, evaporation and transpiration (Law et al., 2015, Sec. 4.1). The difference in LAI will also have an impact on the land carbon fluxes, whereas the impact on the ocean carbon cycle is negligible and therefore our analysis of the ocean carbon fluxes focuses only on one scenario (i.e. PresLAI).

Both configurations of ACCESS-ESM1 were run for 1000 years under pre-industrial climate conditions (year 1850) (Law et al., 2015) with the historical simulations starting from year 800 of these control runs. The historical simulations use external forcing for 1850-2005 such as increasing greenhouse gases, aerosols, changes in solar radiation and volcanic eruptions as used in previous ACCESS versions (Dix et al., 2013). For example, the prescribed atmospheric $CO_2$ increases from 285 $\mathrm{ppm}$ in 1850 to 379 $\mathrm{ppm}$ in 2005.

Volcanic eruptions in ACCESS-ESM1 are prescribed based on monthly global mean stratospheric volcanic aerosol optical depth (Sato et al., 2002) which is then averaged over four equal-area latitude zones, similar to the way it is done in the Hadley Centre Global Environmental Model (HadGEM) (Stott et al., 2006; Jones et al., 2011). Globally significant volcanoes within the historical period are Krakatoa (1883), Santa Maria (1903), Agung (1963), El Chichón (1982) and Pinatubo (1991). Tropospheric aerosols are either calculated interactively (i.e. sea salt and mineral dust) or are based on emission datasets (i.e. sulphate and organic carbon) and increase rapidly from 1950 (Dix et al., 2013, Fig. 4).

The simulations do not include any land-use change; the distribution of PFTs used in the pre-industrial simulation is used throughout the historical period.

### 2.3 Comparison with CMIP5 models

ACCESS-ESM1 is compared against other ESMs that participated in CMIP5 and are available on the Earth System Grid. The models used in this paper are shown in Table 1 with the references provided in Lenton et al. (2015). As not all years were available for these simulations we focused on the period 1870-2005 and used only the first ensemble member for each ESM. In assessing the response of the CMIP5 models, we calculated the median and the 10th and 90th percentiles following Lenton et al. (2015). This allows us to both assess how well ACCESS-ESM1 captures the median and whether it falls into the range of existing CMIP5 models.

### 2.4 Observations

We use the following observational data products to compare against ACCESS-ESM1 outputs. Climate variables are assessed, where this is helpful for interpreting the carbon simulation. For example, the land carbon balance is mainly controlled by surface temperature and precipitation (Piao et al., 2009), whereas the ocean carbon balance is mainly influenced by sea surface temperature (SST) and mixed layer depth (MLD) (Martinez et al., 2009).

*Land surface temperature and precipitation:*Climate Research Unit (CRU) 1901-2013 time-series (TS) data set at version 3.22 (Harris et al., 2014; Jones and Harris, 2014), statistically interpolated to 0.5° x 0.5° from monthly observations at meteoro-

Geosci. Model Dev. Discuss., doi:10.5194/gmd-2016-14, 2016
Manuscript under review for journal Geosci. Model Dev.
Published: 10 May 2016


Geoscientific Model Development Discussions
Open Access
EGU

logical stations across the world's land area (excluding Antarctica). A low resolution version at 5° for land surface temperature anomalies (CRUTEM4, (Jones et al., 2012)) is used for the period 1850-1900.

*Global ocean and land carbon flux:* Global Carbon Project (GCP) estimates of annual global carbon budget components and their uncertainties using a combination of data, algorithms, statistics and model estimates (Le Quéré et al., 2015). The GCP residual land sink is estimated as the difference of emissions from fossil fuel and cement production, emissions from land use and land cover change (LULCC), atmospheric $CO_2$ growth rate and the mean ocean $CO_2$ sink. The 2014 global carbon budget (Le Quéré et al., 2015) provides annual values for the period 1959 to 2013.

*Gross primary production (GPP):* upscaled data from the Flux Network (FLUXNET) using eddy covariance flux data and various diagnostic models (Beer et al., 2010). Gridded data at the global scale is provided by Jung et al. (2011) using a machine learning technique called model tree ensemble (MTE) to scale up FLUXNET observations. Global flux fields are available at a 0.5° x 0.5° spatial resolution and a monthly temporal resolution from 1982 to 2008.

*LAI:* global LAI derived from the third generation (3g) Global Inventory Modeling and Mapping Studies (GIMMS) normalized difference vegetation index (NDVI)3g data set. Neural networks were trained first with best-quality and significantly post-processed Moderate Resolution Imaging Spectroradiometer (MODIS) LAI and Very High Resolution Radiometer (AVHRR) GIMMS NDVI3g data for the overlapping period (2000 to 2009) to derive the final data set at 1/12° resolution and a temporal resolution of 15 days for the period 1981 to 2011 (Zhu et al., 2013).

*Soil organic carbon (SOC):* the Harmonized World Soil Database (HWSD) (FAO, 2012) represents the most comprehensive and detailed globally consistent database of soil characteristics that is currently available for global analysis. We use an upscaled and regridded version of the HWSD with the area weighted SOC calculated from the soil organic carbon (%), bulk density and soil depth (Wieder et al., 2014).

*Atmospheric $CO_2$ concentrations:* mean atmospheric $CO_2$ seasonal cycles derived from NOAA/ESRL flask samples as processed in the GLOBALVIEW (GLOBALVIEW-$CO_2$, 2011) data product. These seasonal cycles are designed to be representative of background, clean-air at any given location. Here, we assess the seasonal cycle for 4 locations with an averaging period of about 20 years for Mace Head (53.33° N, 9.90° W), about 25 years for Alert (82.45° N, 62.52° W), about 35 years for South Pole (89.98° S, 24.80° W) and about 40 years for Mauna Loa (19.53° N, 155.58° W).

*Sea surface temperatures (SST):* the high-resolution (1° x 1°) Hadley SST1 (Rayner et al., 2003) in the period 1870-2006.

*Climatological mixed layer depths:* de Boyer Montégut et al. (2004) for the historical period, based on the density mixed layer criteria of a change density of 0.03 $\mathrm{kg\,m^{-3}}$ from the surface.

*Anthropogenic carbon uptake:* column inventory estimated from Sabine et al. (2004) from GLobal Ocean Data Analysis Project (GLODAP) (Key et al., 2004).

*Sea-air $CO_2$ fluxes:* seasonal climatology of Wanninkhof et al. (2013) based on the 1° x 1° global measurements of oceanic $pCO_2$ of Takahashi et al. (2009).

*Ocean net primary productivity:* net primary productivity from SeaWIFS calculated with the VPGM algorithm of Behrenfeld and Falkowski (1997).

Geosci. Model Dev. Discuss., doi:10.5194/gmd-2016-14, 2016
Manuscript under review for journal Geosci. Model Dev.
Published: 10 May 2016


Geoscientific Model Development Discussions
Open Access
EGU

## 3 ACCESS-ESM1 climatology

### 3.1 Land temperature and precipitation

Carbon fluxes across the historical period will be directly influenced by increasing atmospheric $CO_2$ and indirectly influenced by changes in the climate, driven by the increasing atmospheric $CO_2$ and modulated by other external forcing, such as anthropogenic and volcanic aerosols. In addition, each climate simulation generates its own internal variability, with major modes of climate variability such as the El Niño Southern Oscillation (ENSO) known to generate large variability in carbon exchange between the atmosphere and both the ocean and land (Zeng et al., 2005).

The evolution of temperature and precipitation in ACCESS-ESM1 (Fig. 1) over land shows similar characteristics to ACCESS1.3 historical simulations (Dix et al., 2013; Lewis and Karoly, 2014) as well as those of ACCESS1.4 (P. Vohlarik, pers. comm.). Global land surface air temperature anomalies (relative to 1901-1930) are shown in Fig. 1. Both ACCESS-ESM1 simulation scenarios (PresLAI and ProgLAI) show similar temperature anomalies over most of the historical period, being close to the observed anomalies through most of the period but somewhat lower than observations from 1965-2005. This is attributed by Lewis and Karoly (2014) to a likely overly strong cooling response in ACCESS1.3 to anthropogenic aerosols, offsetting the warming due to greenhouse gas increases for which ACCESS1.3 responds similarly to a CMIP5 mean (Lewis and Karoly, 2014, Figs. 2a, 3a). Strong aerosol cooling is supported by Rotstayn et al. (2015) who found that ACCESS1.3 showed a large global mean aerosol effective radiative forcing (ERF) over the historical period of $-1.56\,\mathrm{Wm}^{-2}$ which is much larger than the IPCC best estimate ($-0.9\,\mathrm{Wm}^{-2}$) (Boucher et al., 2013) but still within the uncertainty range.

Both ACCESS-ESM1 simulations exhibit cooling following major volcanic eruptions (marked in Fig. 1). At first sight, the ProgLAI run seems to be more sensitive to volcanic eruptions, showing a stronger cooling particularly for the two most recent major eruptions, El Chichón in 1982 and Mt. Pinatubo in 1991. However, this difference might be due to a different ENSO phase for the two runs at the time of the eruptions. Lewis and Karoly (2014) assessed the temperature impact of Agung, El Chichón and Pinatubo in three ACCESS1.3 simulations (e.g. their Fig. 7) and mean temperature anomalies from the two ACCESS-ESM1 simulations lie within or only slightly outside the ACCESS1.3 ensemble range. It is worth noting that Lewis and Karoly (2014) found that the simulated temperature anomalies from volcanoes tended to be larger in ACCESS than observed, and this was common across CMIP5 models.

Differences in the year to year temperature anomalies between the two ACCESS-ESM1 scenarios are likely due to internal climate variability. For example, between the years 1940 and 1950, the PresLAI run shows a large negative temperature anomaly and the ProgLAI run shows a positive anomaly. The negative anomaly for the PresLAI is probably related to a strong La Niña event (Nino3 index of -1.2) around the year 1945 (Fig. 1c), whereas in the ProgLAI case we see a small El Niño event (Nino3 index of 0.6) around the same time.

The temperature anomalies hide an absolute temperature difference between the two ACCESS-ESM1 simulations; the ProgLAI scenario produces a slightly warmer climate (0.56 K difference in mean land surface air temperature averaged over 1850-2005) than the PresLAI run. This is consistent with the difference in surface air temperature found for the pre-industrial simulations (Law et al., 2015, Sec. 4.1). As noted in Law et al. (2015) the warmer climate can be explained by the difference in

Geosci. Model Dev. Discuss., doi:10.5194/gmd-2016-14, 2016
Manuscript under review for journal Geosci. Model Dev.
Published: 10 May 2016




LAI, which is generally higher in the prognostic case. This leads to a lower albedo especially for evergreen needleleaf forests during the winter months in the northern hemisphere and consequently to an increase in absorbed radiation. The difference in LAI for both scenarios is explored in more detail in section 5.1.2. Compared to the observations the ACCESS-ESM1 runs show a cooler land surface air temperature by about 0.5 K for the ProgLAI scenario and 1.1 K for the PresLAI scenario averaged over 1901-2005.

Precipitation anomalies over the land are presented in Fig. 1b. Larger differences in the anomalies for the two ACCESS-ESM1 simulations can be observed around the years 1870 to 1880, where the PresLAI scenario shows a positive anomaly and the ProgLAI scenario shows a mainly negative anomaly. The difference over the remaining time period for the two runs is generally small. ACCESS-ESM1 simulations compare well with observed rainfall anomalies until about 1950. After that, observed anomalies are mostly higher than the simulation results, a feature also seen in the ACCESS1.3 historical ensemble (Lewis and Karoly, 2014, Fig. 6a). The comparison of absolute rainfall for the two ACCESS-ESM1 scenarios suggests a dryer climate (approx. 20 $\mathrm{mm\,yr^{-1}}$) for the ProgLAI run.

A reduction in precipitation can be observed following the eruption of major volcanoes for both ACCESS-ESM1 scenarios, apart from the 1982 El Chichón eruption where the PresLAI scenario does not show a strong anomaly and the ProgLAI anomaly is likely too late to be due to the volcano. As for temperature, the precipitation anomalies lie within or close to the ACCESS1.3 ensemble of anomalies presented by Lewis and Karoly (2014, Fig. 9).

### 3.2 Sea surface temperature and mixed layer depth

To assist in the assessment of responses of the ocean net primary productivity (NPP) and sea-air $CO_2$ fluxes, the responses of SST and mixed layer depth are first assessed.

The ocean response from ACCESS-ESM1 is compared with the time series of HadiSST v1 (Rayner et al., 2003). Figure 2. Here we see that the simulated SST does not increase as much as observations over the historical period due a warm bias in the early part of the historical period. This warm bias in ACCESS-ESM1 is the same as reported by Bi et al. (2013) over the period 1870-1899 in ACCESS 1.3 (0.26 K). Followed the observed acceleration in warming in the period 1910-1970, we see ACCESS-ESM1 captures well the observed response of HadiSST in the later period (1970-2005).

However despite little bias in the latter period we see that the ACCESS-ESM1 SST response, consistent with ACCESS 1.3 (Bi et al., 2013), produces very heterogeneous differences from observations. Fig. 3 shows that ACCESS-ESM1 has a strong warm summer bias in SST at the higher latitudes which is weaker but present in the winter. This summer bias is largest in the Southern Ocean where large values are present (>3 K). Away from the higher latitudes, there does not appear to be strong seasonal biases, with the exception of the subtropical North Atlantic which has a coherent bias towards cooler temperatures.

The magnitude of the interannual variability of simulated SST is a similar magnitude as the observations. In response to large aerosol injections associated with volcanic eruptions, overlain on Fig. 2, we see that the ocean does capture a net cooling, as expected (e.g. Stenchikov et al., 2009) and consistent with observations. Interestingly the magnitude of the cooling is sometimes less than observed in HadiSST v1 despite the stronger than observed aerosol response in ACCESS-ESM1.

Geosci. Model Dev. Discuss., doi:10.5194/gmd-2016-14, 2016
Manuscript under review for journal Geosci. Model Dev.
Published: 10 May 2016


Geoscientific Model Development Discussions
Open Access
EGU

Ocean mixed layer depths are compared with the observations from de Boyer Montégut et al. (2004) based on a 0.03 $\mathrm{kg\,m^{-3}}$ density change from the surface. Figure 4 shows that ACCESS-ESM1 appears to slightly overestimate the depth of the winter mixed layers. Winter mixed layers close to or deeper than observed is encouraging given that many ocean models tend to underestimate winter mixed layer depths (Sallée et al., 2013; Downes et al., 2015). At the same time ACCESS-ESM1 appears to underestimate mixed layer depths in the high latitude Southern Ocean in summer. This Southern Ocean underestimate of summer mixed layer depths is consistent with Sallée et al. (2013) who showed that most CMIP5 models tend to underestimate summer mixed layer depths. That this summer bias is also seen in the ocean only version of ACCESS (ACCESS-O Downes et al., 2015) suggests that this bias may be related to the formulation of mixed layer depth in the ocean model, rather than due solely to the summer warming bias. Little bias is seen in summer mixed layers in the higher latitude Northern Hemisphere.

## 4 ACCESS-ESM1 carbon cycle response to historical forcing

The increase in atmospheric $\mathrm{CO_2}$ over the historical period is expected to have a direct impact on both land and ocean carbon fluxes. Additionally there may be indirect impacts from the change in climate caused by the increasing atmospheric $\mathrm{CO_2}$. These impacts are explored firstly for land carbon and then for ocean carbon.

### 4.1 Land carbon response

The direct impact of increasing atmospheric $\mathrm{CO_2}$ is seen clearly in the simulated global land gross primary production (GPP) (Fig. 5a), with increasing GPP for both simulations. The ProgLAI case gives the larger increase, with fluxes for the final 10 years of the simulation being 19% larger than for the first 10 years, compared to an increase of 11% in the PresLAI case. This is due to increasing LAI in the ProgLAI simulation (Fig. 5b) compared to the prescribed LAI which is annually repeating with no increase. Thus the PresLAI case captures only the direct $\mathrm{CO_2}$ fertilisation effect of more efficient photosynthesis per leaf area while the ProgLAI case also allows the growing leaf biomass to increase the global total assimilation. The inter-annual variability (IAV) in GPP over the whole historical period for the ProgLAI run is 2.6 $\mathrm{PgC\,yr^{-1}}$, considerably larger than in the PresLAI case (1.7 $\mathrm{PgC\,yr^{-1}}$), but within the range of other CMIP5 models. We also notice a large decadal variability of global GPP for the ProgLAI case, which is much weaker in the PresLAI case (1.9 vs. 1.3 $\mathrm{PgC\,yr^{-1}}$ ). Natural variability of the climate is the main driver for the IAV in GPP for the PresLAI case. The larger variability in the ProgLAI case is due to the stronger response to volcanic cooling and climate, causing an increase in LAI and a positive feedback through increased GPP. In the PresLAI case, without the LAI feedback, the impact of volcanic cooling is sometimes largely offset by natural climate variability, for example in the Pinatubo (1991) case.

The difference between the two simulations is less obvious for the net ecosystem exchange (Fig. 5c). NEE is a relatively small flux that represents the difference between respiration (heterotrophic and autotrophic) and GPP. In the current set up of ACCESS-ESM1 we do not include disturbances such as fire and LULCC, which means that in this case NEE also represents the net flux of carbon from the land to the atmosphere. Both simulations generally produce small land sinks over most of the historical period, with some tendency to an increasing sink from the 1920s, followed by a possible reduction in the sink from

Geosci. Model Dev. Discuss., doi:10.5194/gmd-2016-14, 2016
Manuscript under review for journal Geosci. Model Dev.
Published: 10 May 2016


Geoscientific Model Development Discussions

the mid 1990s to 2005. The IAV is relatively large and similar for both scenarios (1.4 vs. 1.3 $\mathrm{PgC\,yr^{-1}}$) and likely caused by variations in GPP (Piao et al., 2009; Jung et al., 2011) that are moderated by respiration, especially in the ProgLAI case. Law et al. (2015, Table 2) found similar IAV in the preindustrial simulation with larger GPP IAV in the ProgLAI case offset by positively correlated leaf respiration IAV. Decadal variability for the ProgLAI run is larger than for the PresLAI run (0.7 vs. 0.3 $\mathrm{PgC\,yr^{-1}}$).

Larger decadal variability in the ProgLAI run can be explained by the stronger response to volcanic eruptions. In principle, aerosols scatter incoming solar radiation and therefore have a mainly cooling effect. Hence, an increase in aerosol emissions leads to a decrease in global temperature which in turn increases GPP in the tropics and reduces plant respiration globally in both cases (PresLAI and ProgLAI) and therefore increases NEE. However, whereas in the PresLAI case the LAI is kept at a constant level, in the ProgLAI case the LAI is allowed to increase with the leaf carbon pools (Fig. 5b). This leads to a further increase in GPP at the same time (Fig. 5a) which further increases NEE in the ProgLAI case.

Due to the fact that during the control run NEE did not equilibrate to zero (Law et al., 2015, Sec. 4.2.2), we calculate the carbon uptake for both scenarios by subtracting the mean NEE over the corresponding part of the control run. In this way we estimate a total uptake of carbon to the land over the historical period of 128 $\mathrm{PgC}$ for the PresLAI scenario and 154 $\mathrm{PgC}$ for the ProgLAI scenario. The observation based cumulative historical land carbon uptake is estimated to be $-11 \pm 47$ PgC Arora et al. (2011), which suggests an almost neutral behaviour of the land over that period. Since we do not include disturbances in our model, we do not expect our simulations to match those results. However, we can compare our calculated cumulative uptake against estimates of land-use emissions to see if they are in a similar range. For example, Houghton (2010) reports land-use emissions of 108–188 $\mathrm{PgC}$ for 1850-2000, comparable to the ACCESS-ESM1 cumulative uptakes.

Simulation results from CMIP5 ESMs that include LULCC provide a large range for the total carbon uptake. Shao et al. (2013, Table 4), for example, reports the separate contributions of net ecosystem production (NEP) and disturbance to cumulative land carbon uptake for eight CMIP5 models. While NEP ranges from 24-1730 (median 387) $\mathrm{PgC}$ and disturbance ranges from 3-1729 $\mathrm{PgC}$, the range for land uptake is smaller with two outlying models (-120 and 211 $\mathrm{PgC}$) and the remainder ranging from -59 to 18 $\mathrm{PgC}$. Jones et al. (2013) reports a similar range in land carbon storage across 13 CMIP5 models that include land-use change (-124 to 50 $\mathrm{PgC}$ for 1850-2005). They attribute the wide range to uncertainty in the strength of $\mathrm{CO_2}$ fertilization effects and differences in the way land use change is implemented. The estimates of cumulative NEP from ACCESS-ESM1 are at the low end of the CMIP5 range, possibly due to the inclusion of nitrogen (N) and phosphorus (P) limitation; Zhang et al. (2013) found a reduction of 1850-2005 NEP from 210 $\mathrm{PgC}$ for a carbon-only simulation to 85 $\mathrm{PgC}$ with N and P limitation when using CABLE in a low resolution earth system model.

### 4.2 Ocean response to historical forcing

Figure 6 shows that, consistent with other CMIP5 models, there is no statistically significant trend of ocean NPP globally over the historical period. The global mean NPP from ACCESS-ESM1 of 46 $\mathrm{PgC\,yr^{-1}}$ is close to that calculated from the SeaWIFS data of 52 $\mathrm{PgC\,yr^{-1}}$ for 1998-2005. Furthermore it is also in agreement with estimates, based on observations, of global NPP

Geosci. Model Dev. Discuss., doi:10.5194/gmd-2016-14, 2016
Manuscript under review for journal Geosci. Model Dev.
Published: 10 May 2016


Geoscientific Model Development Discussions

of between 45-50 $\mathrm{PgC\,yr^{-1}}$ (Behrenfeld and Falkowski, 1997). The ACCESS-ESM1 NPP is larger than the median CMIP5 model value of 37 PgC, however NPP in CMIP5 models is associated with a very large range (Anav et al., 2013).

The evolution of sea-air $CO_2$ fluxes in the period 1850-2005 is shown in Fig. 7. Overlain on this plot is the timing of the major volcanic eruptions, the estimated sea-air $CO_2$ flux from the Global Carbon Project (GCP) (Le Quéré et al., 2015) and results from the CMIP5 model archive. Here we see very good agreement with the CMIP5 models in the period 1870-1960, with the ACCESS-ESM1 sitting close to the median of the CMIP5 models, and well within the range of the CMIP5 models. After 1960, ACCESS-ESM1 shows greater uptake than the median of CMIP5 models, and appears to more closely follow the observed value from the GCP, lying at the 10th percentile of the CMIP5 range. For 1960-2005, ACCESS-ESM1 gives a mean sea-air $CO_2$ flux of $1.8 \pm 0.1\,\mathrm{PgC\,yr^{-1}}$ in good agreement with the estimated GCP value of $1.9 \pm 0.3\,\mathrm{PgC\,yr^{-1}}$, and larger than the estimate from CMIP5 models of $1.56 \pm 0.1\,\mathrm{PgC\,yr^{-1}}$. For 1986-2005, the sea-air $CO_2$ is $2.2 \pm 0.1\,\mathrm{PgC\,yr^{-1}}$ from ACCESS-ESM1, the same as from the GCP ($2.2 \pm 0.2\,\mathrm{PgC\,yr^{-1}}$), and larger than the median CMIP5 model value of $1.8 \pm 0.1\,\mathrm{PgC\,yr^{-1}}$. This result highlights that ACCESS-ESM1 show good skill at capturing the globally integrated ocean carbon uptake at the global scale.

## 5 Evaluation of the present day carbon cycle

The last 20 years of the historical simulation (1986-2005) is used to evaluate the simulated carbon cycle against observation based products. Analysis considers the land, ocean and atmosphere in turn.

### 5.1 Land carbon

#### 5.1.1 GPP

Both ACCESS-ESM1 runs (PresLAI and ProgLAI) provide a mean GPP of about $130\,\mathrm{PgC\,yr^{-1}}$ for 1986-2005. The observation based estimate of Jung et al. (2011) suggests a GPP of about $119\,\mathrm{PgC\,yr^{-1}}$ for the same period. Other studies also suggest a global GPP within the same range: Beer et al. (2010) reports an estimate also based on FLUXNET data of $123 \pm 8\,\mathrm{PgC\,yr^{-1}}$ for the period 1998-2005; Ziehn et al. (2011) used plant traits to constrain parameters of the Farquhar photosynthesis model and estimated the global GPP for the same period to be $121\,\mathrm{PgC\,yr^{-1}}$ (95% confidence interval from 110 to $130\,\mathrm{PgC\,yr^{-1}}$) and the IPCC in its AR4 report states a global value of 120 PgC for 1995 (Denman et al., 2007).

The ACCESS-ESM1 simulation results of global GPP agree well with observation based estimates and other studies, although they are somewhat higher. If compared with other CMIP5 earth system models which were divided into two groups by Anav et al. (2013), ACCESS-ESM1 lies in the middle of the lower group with the range 106 to $140\,\mathrm{PgC\,yr^{-1}}$. It was also noted by Anav et al. (2013), that the group of CMIP5 models with a GPP above 150 PgC did not include nitrogen limitation and might therefore overestimate GPP. ACCESS-ESM1 contains both nitrogen and phosphorus limitation, which ensures a more realistic simulation of carbon uptake by the terrestrial biosphere.

Geosci. Model Dev. Discuss., doi:10.5194/gmd-2016-14, 2016
Manuscript under review for journal Geosci. Model Dev.
Published: 10 May 2016


Geoscientific Model Development Discussions
Open Access
EGU

A number of studies that base their estimates on observations suggest that a global GPP of about $120\,\mathrm{PgC\,yr^{-1}}$ may be somewhat too low. For example, Welp et al. (2011) provides a best guess of 150-175 $\mathrm{PgC\,yr^{-1}}$ and (Koffi et al., 2012) an estimate of $146 \pm 19\,\mathrm{PgC\,yr^{-1}}$. However, the estimate by Jung et al. (2011) is based on the largest set of observations and also provides a spatial distribution of GPP. In the following, we therefore use this product for the validation of the ACCESS-ESM1 land carbon component.

The mean annual cycle of GPP as simulated by the ACCESS-ESM1 is shown in Fig. 8 for both scenarios as Anav et al. (2013, Fig. 8). Observation based estimates by Jung et al. (2011) are also shown for comparison. At the global scale both ACCESS-ESM1 runs show a similar behaviour and they both overestimate GPP if compared with the observations as discussed earlier. However, when we split GPP into its contributions from three latitudinal regions we notice larger differences between the two ACCESS-ESM1 simulations. The ProgLAI simulation shows a much more productive northern region and a lower GPP in the tropics which compensate at the global scale. Overall, both ACCESS-ESM1 simulations show good agreement with the observations in terms of the amplitude. In contrast, a large number of CMIP5 models produce a strong positive bias during June-August on a global scale and for the northern hemisphere (Anav et al., 2013). Agreement with observations in terms of the phase is generally good, accept for the Tropics, where ACCESS-ESM1 fails to accurately reproduce the phase. However, as noted by Anav et al. (2013) this is common amongst CMIP5 models.

The spatial distribution of GPP is presented in Fig. 9 along with its IAV for the last 20 years of the historical period. Generally there is good agreement in the spatial pattern of GPP between ACCESS-ESM1 with prescribed LAI and the observation based estimate. However, there are some small differences mainly in tropical regions (i.e. central Africa). The ACCESS-ESM1 ProgLAI run shows a larger GPP in the NH, mostly in the boreal regions, and a lower GPP for large parts of South-America. Comparing the IAV of GPP for the two ACCESS-ESM1 runs reveals large differences. Whereas the PresLAI run shows little variability for most areas, the ProgLAI run shows large hotspots in South-America and Southeast Australia of up to $0.5\,\mathrm{kgC\,m^2\,yr^{-1}}$ which are caused by the LAI feedback as discussed previously. The observation based estimate of GPP shows large areas of variability over the continents, but the distribution and magnitude are quite different to the ACCESS-ESM1 runs. However, as pointed out in Anav et al. (2013) one of the limitations of the GPP observational product is the magnitude of the IAV.

### 5.1.2 LAI

Global LAI estimates are mainly derived from satellite observations and various products are available. The prescribed LAI in ACCESS-ESM1 is based on MODIS observations (Yang et al., 2006) with no IAV. If compared with the observation based estimates of Zhu et al. (2013), which uses a combination of MODIS and AVHRR data, over the last 20 years of the historical period (mean of 1.4), we notice that our current prescribed LAI is somewhat smaller (mean of 1.3), but agrees well in terms of its seasonal cycle (Fig. 10). There is a number of reasons why remote sensing LAI products differ from each other, i.e. because different sensors and algorithms are used (Los et al., 2000).

The prognostic LAI which is calculated by CASA-CNP is significantly higher at the global scale (mean: 1.7) and also shows a different seasonality with its peak in August, whereas the observations suggest the peak is in July (Fig. 10). In CABLE the

Geosci. Model Dev. Discuss., doi:10.5194/gmd-2016-14, 2016
Manuscript under review for journal Geosci. Model Dev.
Published: 10 May 2016




phenology phase is currently prescribed and the leaf onset might be defined as too late for deciduous vegetation which leads to a shift in the LAI peak by about one month.

The global seasonal cycle of LAI is mainly influenced by the northern extra-tropics and we notice that leaf coverage throughout the year and especially in autumn and winter is too high in the ProgLAI case. We clearly overestimate the mean LAI (observations suggest a mean of 1.3) and underestimate the seasonal variability. On a PFT level the main contributor to this is evergreen needle leaf forest which produces a large value (mean 3.8) over the whole year with only a very small seasonal cycle. In the tropics we underestimate LAI by a significant amount (mean of 1.5 in comparison to 2.3 as suggested by observations). This is mainly due to C4 grass showing an LAI which is about a factor of 5 smaller than the observations. Law et al. (2015) attributes the low simulated LAI of C4 grass to a large sensitivity to rainfall and the inability of CABLE to grow back C4 grass after a die back.

The overestimation of the LAI for evergreen needle leaf forest and the underestimation for C4 grass have a direct impact on GPP, which is also too large for evergreen needle leaf and too low for C4 grass. In CABLE, the calculation of GPP is related to APAR (absorbed photosynthetic active radiation) which is the product of FPAR (fraction of photosynthetically active radiation ) and PAR (photosynthetically active radiation) with FPAR calculated from the LAI.

At the global scale, most CMIP5 earth system models also tend to overestimate LAI (Anav et al., 2013, Fig. 11), ranging from 1.5 in December-January to almost 3.5 in June-August. Anav et al. (2013) reports that only 2 models captured the main feature of the global LAI pattern, whereas the remaining 16 models overestimate the global LAI with some even exceeding a mean of 2.4. At the regional scale the ACCESS-ESM1 prognostic LAI is within the CMIP5 range for both hemispheres, but below the CMIP5 range for the Tropics.

#### 5.1.3 NEE

We compare our NEE results against estimates of the residual land sink from the global carbon project (GCP) (Le Quéré et al., 2015) for 1959–2005 (Fig. 5c). The mean residual land sink and interannual variability for this period is estimated to be about $1.9\pm1.0\ \mathrm{PgCy}^{-1}$ compared to $1.4\pm1.3\ \mathrm{PgCy}^{-1}$ for PresLAI and $1.8\pm1.6\ \mathrm{PgCy}^{-1}$ for ProgLAI. In all cases the IAV is large relative to the mean uptake, but more so in the ACCESS-ESM1 simulations. The large IAV makes it difficult to be definitive about land uptake trends over this period, though there is some suggestion of slightly increasing uptake in the GCP budget estimates but slightly decreasing uptake in the ACCESS-ESM1 simulations. This might be better assessed using an ensemble of simulations and extending the analysis closer to 2015 through use of the RCP scenario simulations. Simulations without anthropogenic aerosols would also be useful to determine whether the relatively strong cooling due to tropospheric aerosols in ACCESS-ESM1 is impacting the decadal evolution of land carbon uptake.

#### 5.1.4 CNP pool sizes

The amount of carbon, nitrogen and phosphorus stored in the biomass and soil of terrestrial ecosystems as simulated by ACCESS-ESM1 is compared against other estimates from the literature. Here, we refer to the terrestrial biomass as the sum of

Geosci. Model Dev. Discuss., doi:10.5194/gmd-2016-14, 2016
Manuscript under review for journal Geosci. Model Dev.
Published: 10 May 2016




living above ground (leaf and wood) and below ground (roots) material. All mean pool sizes and spatial distributions derived from ACCESS-ESM1 are calculated over the last 20 years of the historical period (1986-2005).

Carbon pool sizes simulated with ACCESS-ESM1 are in general smaller for the PresLAI scenario as shown in Table 2. The total carbon in the terrestrial biomass amounts to 670 PgC (PresLAI) and 807 PgC (ProgLAI). The IPCC (Prentice et al., 2001) reports two different estimates of 466 PgC and 654 PgC for the global plant carbon stock, depending on the data being used. This would imply that our plant carbon pools are somewhat to large, especially for the ProgLAI scenario. However, other studies such as Houghton et al. (2009) suggest a range of 800-1300 PgC for the global terrestrial biomass. The large range is a result of inconsistent definitions of forest, uncertain estimates of forest area, paucity of ground measurements and the lack of reliable mechanisms for upscaling ground measurements to larger areas (Houghton et al., 2009).

A large number of observational based estimates for global soil organic carbon (SOC) exists with most studies reporting a global estimate of about 1500 PgC (Scharlemann et al., 2014). SOC pools simulated by ACCESS-ESM1 are somewhat smaller with 1050 PgC for the PresLAI scenario and about 1200 PgC for the ProgLAI scenario. However, these numbers agree well with the best estimate of 1260 PgC derived from the HWSD (FAO, 2012) and considering the large range of 510 - 3040 PgC of global SOC simulated by CMIP5 models (Todd-Brown et al., 2013) this is an encouraging results.

The Harmonized World Soil Database (HWSD) also provides a spatial distribution of the SOC density which is shown in Fig.11 along with the results from ACCESS-ESM1. In general there is good agreement between the two ACCESS-ESM1 scenarios, showing a similar pattern, but with a slightly larger density in the NH boreal region for the ProgLAI run. The agreement between the HWSD and ACCESS-ESM1 is also generally good. However, the HWSD suggest localized hot spots of high SOC density in North America and Siberia which are not covered by ACCESS-ESM1. We also underestimate SOC in the tropics especially in the maritime continent region. On the other hand, both ACCESS-ESM1 scenarios suggest a high SOC density in the north Asian region, which is not apparent in the HWSD.

In addition to other environmental constraints such as water, light and temperature, carbon storage by terrestrial ecosystems may also be limited by nutrients, predominantly nitrogen and phosphorus (Wang and Houlton, 2009; Wang et al., 2010; Zhang et al., 2013). However, few estimates are available of total nitrogen and phosphorus pool sizes and their global spatial distribution is even more uncertain.

Simulated nitrogen pool sizes are shown in Table 2 and there is only a small difference between the two ACCESS-ESM1 scenarios. Our estimate for the nitrogen in the terrestrial biomass is about 6.5 PgN. Estimates based on field data reconstructions range from about 3.5 PgN (Schlesinger, 1997) to 10 PgN (Davidson, 1994) which places the ACCESS-ESM1 results right in the middle of that range. Soil organic nitrogen pools are simulated to be about 85 PgN for both ACCESS-ESM1 scenarios which is slightly low if compared with estimates based on field data (95 PgC (Post et al., 1985) to 140 PgC (Batjes, 1996)).

The terrestrial phosphorus cycle at present day is even less constrained than the nitrogen cycle and modelling and empirical estimates vary greatly. ACCESS-ESM1 results suggest a total of 0.35 PgP in the terrestrial biosphere which is slightly lower than the estimated range of 0.5 - 1 PgP by Smil (2000). Organic soil phosphorus pool sizes differ to some extent between the two ACCESS-ESM1 scenarios. The PresLAI model run simulates a pool size of about 10 PgP and the ProgLAI model run

Geosci. Model Dev. Discuss., doi:10.5194/gmd-2016-14, 2016
Manuscript under review for journal Geosci. Model Dev.
Published: 10 May 2016


Geoscientific Model Development Discussions
Open Access
EGU

gives a pool size of about 12 PgP (see Table 2). Other estimates range from about 5 PgP to about 200 PgP with the upper end being assessed as unrealistic (Smil, 2000).

### 5.2 Ocean carbon

#### 5.2.1 Net primary production

To assess the NPP response in different latitude bands, the global ocean is broken down into 5 regions, following Anav et al. (2013). Figure 13 shows NPP seasonal anomaly from ACCESS-ESM1, CMIP5 models and SeaWIFS. Seasonally, at the global ocean scale, we see that the NPP from ACCESS-ESM1 is less than the amplitude of CMIP5 and SeaWIFS, with poor phasing. This likely reflects the biases in ACCESS-ESM1 toward lower latitudes, reflecting excess nutrient supply and utilization to the upper oligotrophic ocean (Law et al., 2015).

In the northern and southern subtropical gyres ACCESS-ESM1 appears to overestimate the amplitude of the observed seasonal cycle when compared with SeaWIFS. In the northern subtropical gyre ACCESS-ESM1 appears to lag by up to 3 months compared with SeaWIFS and CMIP5, which show good agreement. However in the southern subtropical gyre, there is poor agreement in the phasing between ESM (ACCESS-ESM1 and CMIP5) and SeaWIFS, which are two months ahead (CMIP5) and two months behind (ACCESS-ESM1) respectively. In the high latitude northern hemisphere the amplitude of ACCESS-ESM1, consistent with other ESMs (CMIP5), underestimates the amplitude of the seasonal cycle. Again the phase of the seasonal cycle is delayed in ACCESS-ESM1 by up to two months relative to SeaWIFS, but is quite different from other ESMs (CMIP5) which proceed SeaWIFS by up to 2months. In the high latitude Southern Ocean, the magnitude of the seasonal cycle is reproduced well in ACCESS-ESM1, as opposed to CMIP5 ESMs. However the phase of ACCESS-ESM1 appears to be delayed by several months. Finally in the tropical ocean we see very good agreement in the amplitude of the seasonal cycle with CMIP5 and SeaWIFS. We note that comparing the phase of the seasonal cycle from ESMs (ACCESS-ESM1 and CMIP5) with SeaWIFS is not very meaningful as they all simulate their own ENSO cycle with their own timing. Therefore any comparison over a 20 year period between models has the potential to be biased by the number of El Niño or La Niña events.

#### 5.2.2 Sea-air $CO_2$ fluxes

Figure 12 shows that, in the period 1986-2005, ACCESS-ESM1 is in good agreement with the spatial pattern and the magnitude of sea-air $CO_2$ fluxes of Wanninkhof et al. (2013), hereafter referred to as W13. In the Southern Ocean (44 S-90 S), which is an important net sink of carbon, ACCESS-ESM1 (-0.77 $\mathrm{PgC\,yr^{-1}}$) captures a larger annual mean uptake than the sea-air $CO_2$ flux of W13 who only estimated an uptake of -0.18 $\mathrm{PgC\,yr^{-1}}$. In the Southern subtropical gyres (44 S-18 S) ACCESS-ESM1 (-0.39 $\mathrm{PgC\,yr^{-1}}$) captures, but overestimates, the observed sea-air flux of W13 (-0.23 $\mathrm{PgC\,yr^{-1}}$). In contrast in the Northern Hemisphere ACCESS-ESM1 underestimates the uptake at -0.36 $\mathrm{PgC\,yr^{-1}}$ and -0.19 $\mathrm{PgC\,yr^{-1}}$ in the subtropical, and (sub) polar regions respectively, while W13 estimated the uptake at -0.69 $\mathrm{PgC\,yr^{-1}}$ and -0.54 $\mathrm{PgC\,yr^{-1}}$ over the same regions. The uptake in the tropical ocean is well captured, showing very good agreement between ACESS-ESM1 and W13 who estimate

Geosci. Model Dev. Discuss., doi:10.5194/gmd-2016-14, 2016
Manuscript under review for journal Geosci. Model Dev.
Published: 10 May 2016


Geoscientific Model Development Discussions
Open Access
EGU

an uptake of -0.56 $\mathrm{PgC\,yr^{-1}}$ and -0.57 $\mathrm{PgC\,yr^{-1}}$. Spatially the interannual variability in sea-air $CO_2$ flux is presented in a companion paper (Law et al., 2015).

The anomaly of the seasonal cycle of the sea-air $CO_2$ fluxes were assessed against observations of W13 and CMIP5, shown in Fig.14. ACCESS-ESM1 shows that globally the amplitude of the sea-air $CO_2$ fluxes appears larger than observed (W13) and CMIP5 models. Furthermore it appears that globally the phase of sea-air $CO_2$ fluxes are not well captured in ACCESS-ESM1, explaining why it lies outside the range of the CMIP5 models. Many of these global differences are due to representation of the Southern Ocean in ACCESS-ESM1, which does not capture well the amplitude nor phase of the seasonal cycle. This inability to reproduce the observed response may well reflect the strong summer bias in warming, and the subsequent limited NPP in this region. This suggests that during the summer the solubility response likely dominates over the NPP response, leading to an out-gassing in the summer and uptake in the winter, as discussed in Lenton et al. (2013). In the high latitude Northern Hemisphere, the seasonal cycle of sea-air $CO_2$ fluxes in ACCESS-ESM1 appears also to be larger than W13, but within the range of CMIP5 models.

ACCESS-ESM1 appears to capture well the phase of sea-air $CO_2$ fluxes in the subtropical gyres. In the northern subtropical gyre, we see that the amplitude and phase of the seasonal cycle in ACCESS-ESM1 shows very good agreement with W13, in constrast with other ESMs (CMIP5). In the southern subtropical gyres, while the ACCESS-ESM1 appears to overestimate the amplitude, we see very good agreement with CMIP5 models. As anticipated the tropical ocean shows very little seasonality, nevertheless we do see good agreement with CMIP5 models. However the comparison of ACCESS-ESM1 against observations (while shown) is not very meaningful as W13 is based on values of oceanic $pCO_2$ from Takahashi et al. (2009) which does not include El Niño years.

#### 5.2.3 Anthropogenic inventory

The global inventory of anthropogenic carbon from ACCESS-ESM1 is compared with the uptake from GLODAP (Sabine et al., 2004) for the year 1994 in Fig. 15. Here we see that the spatial pattern of the column inventory of anthropogenic carbon is very well reproduced with the large storage occurring in the North Atlantic and large uptake in the Southern Ocean. The inventory for the period 1850–1994 in ACCESS-ESM1 is 130 PgC, which is close to the estimated value from GLODAP of $118 \pm 19$ PgC. This suggests that despite a somewhat limited representation of the seasonal cycle of sea-air $CO_2$ fluxes in key regions of anthropogenic uptake such as the Southern Ocean, that ACCESS-ESM1 is doing a very good job, spatially and temporally, of capturing and storing anthropogenic carbon.

### 5.3 Atmospheric $CO_2$

The land and ocean carbon fluxes have been put into two atmospheric tracers as described in Law et al. (2015, Sec. 2.4). These tracers have no impact on the model simulation but allow the atmospheric $CO_2$ distribution to be assessed. A reasonable simulation of known features of atmospheric $CO_2$ can increase our confidence in the simulated carbon fluxes. For example the seasonal cycle of atmospheric $CO_2$ is strongly driven by the seasonality in land carbon fluxes.

Therefore, our simulated seasonality can be realistically compared to present day atmospheric $CO_2$ observations.

Geosci. Model Dev. Discuss., doi:10.5194/gmd-2016-14, 2016
Manuscript under review for journal Geosci. Model Dev.
Published: 10 May 2016


Geoscientific Model Development Discussions

The seasonal cycle of atmospheric $CO_2$ is shown for four locations at different latitudes (Fig. 16, note the different vertical scale in the upper and lower panels). Seasonal cycles from the PresLAI and ProgLAI cases are calculated as the mean over the last 20 years of the historical period (1986-2005) with the annual mean removed from each year. The seasonality is plotted for the contribution from the land carbon fluxes only and for both the land and ocean carbon fluxes combined. The model output was taken from the nearest grid point to each location with the exception of Mace Head, where the model was sampled further west to better approximate the observations which are selected for clean-air (ocean) conditions.

As observed the amplitude of the seasonal cycle decreases from north to south. At Alert (82° N, Fig.16(a)) both model simulations overestimate the seasonal amplitude with the growing season starting earlier than currently observed. The ocean carbon fluxes contribute little to seasonality at this latitude. At Mace Head (53° N, Fig.16(b)) the simulated seasonal cycle is comparable to that observed while at Mauna Loa (20° N,Fig.16(c)) the ProgLAI case better represents the observed seasonality than the PresLAI case.

Seasonal cycles in the southern hemisphere (e.g. South Pole) are more challenging to simulate correctly as they are made up of roughly equal contributions from local land fluxes, northern hemisphere land fluxes and ocean fluxes. Figure16(d) shows for the PresLAI case that the simulated seasonality from the land carbon fluxes is shifted in phase when the ocean carbon contribution is included but the phase shift is away from the observed seasonality. This phase shift is not apparent for the case with ProgLAI.

## 6 Conclusions

The evaluation of ACCESS-ESM1 over the historical period is an essential step before using the model to predict future uptake of carbon by land and oceans. Here, we performed two different scenarios for the evaluation of the land carbon cycle: running ACCESS-ESM1 with a prescribed LAI and a prognostic LAI. Running with a prognostic LAI is our preferred choice, since this includes the vegetation feedback through the coupling between LAI and the leaf carbon pool. However, results have shown that we overestimate the amplitude of the prognostic LAI annual cycle in the northern and southern hemisphere, and underestimate it in the tropics. In future versions we need to improve the performance of the prognostic LAI, particularly for evergreen needle leaf and C4 grass.

ACCESS-ESM1 shows a strong cooling response to anthropogenic aerosols, which is offsetting the warming due to increases in greenhouse gases. The aerosol radiative forcing over the historical period is much stronger than the IPCC best estimate, but still within the uncertainty range. The impact of the cooling due to anthropogenic aerosols in ACCESS-ESM1 needs to be quantified in future work.

The land carbon uptake over the historical period is by about $20\%$ larger for the run with prognostic LAI in comparison to the run with prescribed LAI. This is mainly due to the stronger response to volcanic eruptions which increases GPP in the tropics and reduces plant respiration globally and therefore increases NEE.

Simulated carbon pool sizes are generally within the range of estimates provided in the literature. Simulated soil organic carbon has been compared against the Harmonized World Soil Database, finding very good agreement in the spatial distribution

Geosci. Model Dev. Discuss., doi:10.5194/gmd-2016-14, 2016
Manuscript under review for journal Geosci. Model Dev.
Published: 10 May 2016




and the total size. Nitrogen and phosphorus limitation were active in our simulations and pool sizes seem reasonable if compared with other estimates. However, nitrogen and phosphorus cycles are poorly constrained and only a few global estimates exist with large uncertainties.

ACCESS-ESM1 has the capability of putting land and ocean carbon fluxes into tracers which provides a way of assessing simulated atmospheric $CO_2$ concentrations. The simulated seasonal cycle is close to the observed, but we overestimate the amplitude in the high northern latitude and we also notice small phase shifts.

Globally integrated sea-air $CO_2$ fluxes are well reproduced, capturing well the most recent observations of the Global Carbon Project (Le Quéré et al., 2015) and anthropogenic uptake of Sabine et al. (2004); Key et al. (2004). The spatial distribution of sea-air $CO_2$ fluxes is also well reproduced. Seasonally the ACCESS-ESM1 appears biased toward the Southern Hemisphere with too much uptake and too little in the North, while the tropics are well captured. These differences appear to be strongly related to the dynamical response of the model. Nevertheless in most regions the results of ACCESS-ESM1 lie within the range of published CMIP5 ESMs. Globally the annual mean ocean NPP is well captured, but is somewhat biased to the low latitudes, when compared with observations, reflecting excess nutrient delivery to the lower latitude ocean in ACCESS-ESM1.

Overall, land and ocean carbon modules provide realistic simulations of land and ocean carbon exchange, suggesting that ACCESS-ESM1 is a valuable tool to explore the change in land and oceanic uptake in the future.

## Code availability

Code availability varies for different components of ACCESS-ESM1. The UM is licensed by the UK Met Office and is not freely available. CABLE2 is available from https://trac.nci.org.au/svn/cable/. See https://trac.nci.org.au/trac/cable/wiki/CableRegistration for information on registering to use the CABLE repository. MOM4p1 and CICE are freely available under applicable registration or copyright conditions. For MOM4p1 see http://data1.gfdl.noaa.gov/~arl/pubrel/r/mom4p1/src/mom4p1/doc/mom4_manual.html. For CICE see http://oceans11.lanl.gov/trac/CICE. For access to the MOM4p1 code with WOMBAT as used for ACCESS-ESM1, please contact Hailin Yan (Hailin.Yan@csiro.au). The OASIS3-MCT 2.0 coupler code is available from http://oasis.enes.org.

*Acknowledgements.* This research is supported by the Australian Government Department of the Environment, the Bureau of Meteorology and CSIRO through the Australian Climate Change Science Programme. The research was undertaken on the NCI National Facility in Canberra, Australia, which is supported by the Australian Commonwealth Government. The authors wish to acknowledge use of the Ferret program for some of the analysis and graphics in this paper. Ferret is a product of NOAA's Pacific Marine Environmental Laboratory. (Information is available at http://ferret.pmel.noaa.gov/Ferret/). We acknowledge the World Climate Research Programme's Working Group on Coupled Modelling, which is responsible for CMIP, and we thank the climate modelling groups (listed in Table 1 of this paper) for producing and making available their model output. For CMIP the U.S. Department of Energy's Program for Climate Model Diagnosis and Intercomparison provides coordinating support and led development of software infrastructure in partnership with the Global Organization for Earth System Science Portals.

Geosci. Model Dev. Discuss., doi:10.5194/gmd-2016-14, 2016
Manuscript under review for journal Geosci. Model Dev.
Published: 10 May 2016




## References

Anav, A., Friedlingstein, P., Kidston, M., Bopp, L., Ciais, P., Cox, P., Jones, C., Jung, M., Myneni, R., and Zhu, Z.: Evaluating the Land and Ocean Components of the Global Carbon Cycle in the CMIP5 Earth System Models, J. Climate, 26, 6801–6843, 2013.

Arora, V. K., Scinocca, J. F., Boer, G. J., Christian, J. R., Denman, K. L., Flato, G. M., Kharin, V. V., Lee, W. G., and Merryfield, W. J.: Carbon emission limits required to satisfy future representative concentration pathways of greenhouse gases, Geophysical Research Letters, 38, n/a–n/a, doi:10.1029/2010GL046270, http://dx.doi.org/10.1029/2010GL046270, l05805, 2011.

Arora, V. K., Boer, G. J., Friedlingstein, P., Eby, M., Jones, C. D., Christian, J. R., Bonan, G., Bopp, L., Brovkin, V., Cadule, P., Hajima, T., Ilyina, T., Lindsay, K., Tjiputra, J. F., and Wu, T.: Carbon-Concentration and Carbon-Climate Feedbacks in CMIP5 Earth System Models, J. Climate, 26, 5289–5314, 2013.

Batjes, N.: Total carbon and nitrogen in the soils of the world, European Journal of Soil Science, 47, 151–163, doi:10.1111/j.1365-2389.1996.tb01386.x, http://dx.doi.org/10.1111/j.1365-2389.1996.tb01386.x, 1996.

Beer, C., Reichstein, M., Tomelleri, E., Ciais, P., Jung, M., Carvalhais, N., Rödenbeck, C., Arain, M. A., Baldocchi, D., Bonan, G. B., Bondeau, A., Cescatti, A., Lasslop, G., Lindroth, A., Lomas, M., Luyssaert, S., Margolis, H., Oleson, K. W., Roupsard, O., Veenendaal, E., Viovy, N., Williams, C., Woodward, F. I., and Papale, D.: Terrestrial Gross Carbon Dioxide Uptake: Global Distribution and Covariation with Climate, Science, 329, 834–838, doi:10.1126/science.1184984, http://www.sciencemag.org/content/329/5993/834.abstract, 2010.

Behrenfeld, M. J. and Falkowski, P. G.: Photosynthetic rates derived from satellite-based chlorophyll concentration, Limnology and Oceanography, 42, 1–20, doi:10.4319/lo.1997.42.1.0001, http://dx.doi.org/10.4319/lo.1997.42.1.0001, 1997.

Bi, D., Dix, M., Marsland, S. J., O'Farrell, S., Rashid, H. A., Uotila, P., Hirst, A. C., Kowalczyk, E., Golebiewski, M., Sullivan, A., Yan, H., Hannah, N., Franklin, C., Sun, Z., Vohralik, P., Watterson, I., Zhou, X., Fiedler, R., Collier, M., Ma, Y., Noonan, J., Stevens, L., Uhe, P., Zhu, H., Griffies, S. M., Hill, R., Harris, C., and Puri, K.: The ACCESS coupled model: description, control climate and evaluation, Aus. Meteor. Oceanogr. J., 63, 41–64, 2013.

Booth, B. B. B., Jones, C. D., Collins, M., Totterdell, I. J., Cox, P. M., Sitch, S., Huntingford, C., Betts, R. A., Harris, G. R., and Lloyd, J.: High sensitivity of future global warming to land carbon cycle processes, Environmental Research Letters, 7, 024 002, http://stacks.iop.org/1748-9326/7/i=2/a=024002, 2012.

Boucher, O., Randall, D., Artaxo, P., Bretherton, C., Feingold, G., Forster, P., Kerminen, V.-M., Kondo, Y., Liao, H., Lohmann, U., Rasch, P., Satheesh, S. K., Sherwood, S., Stevens, B., and Zhang, X.: Clouds and Aerosols, book section 7, p. 571–658, Cambridge University Press, Cambridge, United Kingdom and New York, NY, USA, doi:10.1017/CBO9781107415324.016, www.climatechange2013.org, 2013.

Davidson, E.: Climate Change and Soil Microbial Processes: Secondary Effects are Hypothesised from Better Known Interacting Primary Effects, in: Soil Responses to Climate Change, edited by Rounsevell, M. and Loveland, P., vol. 23 of *NATO ASI Series*, pp. 155–168, Springer Berlin Heidelberg, doi:10.1007/978-3-642-79218-2_10, http://dx.doi.org/10.1007/978-3-642-79218-2_10, 1994.

de Boyer Montégut, C., Madec, G., Fischer, A. S., Lazar, A., and Iudicone, D.: Mixed layer depth over the global ocean: An examination of profile data and a profile-based climatology, Journal of Geophysical Research: Oceans, 109, n/a–n/a, doi:10.1029/2004JC002378, http://dx.doi.org/10.1029/2004JC002378, c12003, 2004.

Denman, K. L., Brasseur, G., Chidthaisong, A., Ciais, P., Cox, P. M., Dickinson, R. E., Hauglustaine, D., Heinze, C., Holland, E., Jacob, D., Lohmann, U., Ramachandran, S., Dias, Wofsy, S. C., and Zhang, X.: Couplings Between Changes in the Climate System and Biogeochemistry, in: Climate Change 2007: The Physical Science Basis. Contribution of Working Group I to the Fourth Assessment Report



of the Intergovernmental Panel on Climate Change, edited by Solomon, S., Qin, D., Manning, M., Chen, Z., Marquis, M., Averyt, K. B., Tignor, M., and Miller, H. L., Cambridge University Press, Cambridge, UK and New York, NY, 2007.

Dix, M., Vohralik, P., Bi, D., Rashid, H., Marsland, S., O'Farrell, S., Uotila, P., Hirst, T., Kowalczyk, E., Sullivan, A., Yan, H., Franklin, C., Sun, Z., Watterson, I., Collier, M., Noonan, J., Rotstayn, L., Stevens, L., Uhe, P., and Puri, K.: The ACCESS coupled model: documentation of core CMIP5 simulations and initial results, Aus. Meteor. Oceanogr. J., 63, 83–99, 2013.

Downes, S. M., Farneti, R., Uotila, P., Griffies, S. M., Marsland, S. J., Bailey, D., Behrens, E., Bentsen, M., Bi, D., Biastoch, A., Böning, C., Bozec, A., Canuto, V. M., Chassignet, E., Danabasoglu, G., Danilov, S., Diansky, N., Drange, H., Fogli, P. G., Gusev, A., Howard, A., Ilicak, M., Jung, T., Kelley, M., Large, W. G., Leboissetier, A., Long, M., Lu, J., Masina, S., Mishra, A., Navarra, A., Nurser, A. G., Patara, L., Samuels, B. L., Sidorenko, D., Spence, P., Tsujino, H., Wang, Q., and Yeager, S. G.: An assessment of Southern Ocean water masses and sea ice during 1988–2007 in a suite of interannual CORE-II simulations, Ocean Modelling, 94, 67 – 94, doi:http://dx.doi.org/10.1016/j.ocemod.2015.07.022, http://www.sciencedirect.com/science/article/pii/S1463500315001420, 2015.

FAO: Harmonized World Soil Database (version 1.2), fAO/IIASA/ISRIC/ISSCAS/JRC, 2012.

Friedlingstein, P., Cox, P., Betts, R., Bopp, L., von Bloch, W., Brovkin, V., Cadule, P., Doney, S., Eby, M., Fung, I., Bala, G., John, J., Jones, C., Joos, F., Kato, T., Kawamiya, M., Knorr, W., Lindsay, K., Matthews, H. D., Raddatz, T., Rayner, P., Reick, C., Roeckner, E., Schnitzler, K.-G., Schnur, R., Strassmann, K., Weaver, A. J., Yoshikawa, C., and Zeng, N.: Climate–carbon cycle feedback analysis: results from the $C^4$MIP model intercomparison, J. Climate, 19, 3337–3353, doi:10.1175/JCLI3800.1, 2006.

Friend, A. D., Lucht, W., Rademacher, T. T., Keribin, R., Betts, R., Cadule, P., Ciais, P., Clark, D. B., Dankers, R., Falloon, P. D., Ito, A., Kahana, R., Kleidon, A., Lomas, M. R., Nishina, K., Ostberg, S., Pavlick, R., Peylin, P., Schaphoff, S., Vuichard, N., Warszawski, L., Wiltshire, A., and Woodward, F. I.: Carbon residence time dominates uncertainty in terrestrial vegetation responses to future climate and atmospheric CO2, Proceedings of the National Academy of Sciences, 111, 3280–3285, doi:10.1073/pnas.1222477110, http://www.pnas.org/content/111/9/3280.abstract, 2014.

Frölicher, T. L., Sarmiento, J. L., Paynter, D. J., Dunne, J. P., Krasting, J. P., and Winton, M.: Dominance of the Southern Ocean in anthropogenic carbon and heat uptake in CMIP5 models, Journal of Climate, 28, 862–886, 2015.

GLOBALVIEW-$CO_2$: Cooperative Atmospheric Data Integration Project - Carbon Dioxide, www.esrl.noaa.gov/gmd/ccgg/globalview/co2/co2_version.html, nOAA ESRL, Boulder, Colorado, 2011.

Goll, D. S., Brovkin, V., Parida, B. R., Reick, C. H., Kattge, J., Reich, P. B., van Bodegom, P. M., and Niinemets, U.: Nutrient limitation reduces land carbon uptake in simulations with a model of combined carbon, nitrogen and phosphorus cycling, Biogeosciences, 9, 3547–3569, doi:10.5194/bg-9-3547-2012, http://www.biogeosciences.net/9/3547/2012/, 2012.

Harris, I., Jones, P., Osborn, T., and Lister, D.: Updated high-resolution grids of monthly climatic observations – the CRU TS3.10 Dataset, International Journal of Climatology, 34, 623–642, doi:10.1002/joc.3711, http://dx.doi.org/10.1002/joc.3711, 2014.

Houghton, R. A.: How well do we know the flux of CO2 from land-use change?, Tellus B, 62, 337–351, doi:10.1111/j.1600-0889.2010.00473.x, http://dx.doi.org/10.1111/j.1600-0889.2010.00473.x, 2010.

Houghton, R. A., Hall, F., and Goetz, S. J.: Importance of biomass in the global carbon cycle, Journal of Geophysical Research: Biogeosciences, 114, n/a–n/a, doi:10.1029/2009JG000935, http://dx.doi.org/10.1029/2009JG000935, g00E03, 2009.

Jones, C., Robertson, E., Arora, V., Friedlingstein, P., Shevliakova, E., Bopp, L., Brovkin, V., Hajima, T., Kato, E., Kawamiya, M., Liddicoat, S., Lindsay, K., Reick, C. H., Roelandt, C., Segschneider, J., and Tjiputra, J.: Twenty-First-Century Compatible CO2 Emissions and Airborne Fraction Simulated by CMIP5 Earth System Models under Four Representative Concentration Pathways, J. Climate, 26, 4398–4413, doi:10.1175/jcli-d-12-00554.1, http://dx.doi.org/10.1175/jcli-d-12-00554.1, 2013.



Jones, C. D., Hughes, J. K., Bellouin, N., Hardiman, S. C., Jones, G. S., Knight, J., Liddicoat, S., O'Connor, F. M., Andres, R. J., Bell, C., Boo, K.-O., Bozzo, A., Butchart, N., Cadule, P., Corbin, K. D., Doutriaux-Boucher, M., Friedlingstein, P., Gornall, J., Gray, L., Halloran, P. R., Hurtt, G., Ingram, W. J., Lamarque, J.-F., Law, R. M., Meinshausen, M., Osprey, S., Palin, E. J., Parsons Chini, L., Raddatz, T., Sanderson, M. G., Sellar, A. A., Schurer, A., Valdes, P., Wood, N., Woodward, S., Yoshioka, M., and Zerroukat, M.: The HadGEM2-ES implementation of CMIP5 centennial simulations, Geoscientific Model Development, 4, 543–570, doi:10.5194/gmd-4-543-2011, http://www.geosci-model-dev.net/4/543/2011/, 2011.

Jones, P. and Harris, I.: CRU TS3.22: Climatic Research Unit (CRU) Time-Series (TS) Version 3.22 of High Resolution Gridded Data of Month-by-month Variation in Climate (Jan. 1901- Dec. 2013), doi:doi:10.5285/18BE23F8-D252-482D-8AF9-5D6A2D40990C, http://dx.doi.org/10.5285/18BE23F8-D252-482D-8AF9-5D6A2D40990C, 2014.

Jones, P. D., Lister, D. H., Osborn, T. J., Harpham, C., Salmon, M., and Morice, C. P.: Hemispheric and large-scale land-surface air temperature variations: An extensive revision and an update to 2010, Journal of Geophysical Research: Atmospheres, 117, n/a–n/a, doi:10.1029/2011JD017139, http://dx.doi.org/10.1029/2011JD017139, d05127, 2012.

Jung, M., Reichstein, M., Margolis, H. A., Cescatti, A., Richardson, A. D., Arain, M. A., Arneth, A., Bernhofer, C., Bonal, D., Chen, J., Gianelle, D., Gobron, N., Kiely, G., Kutsch, W., Lasslop, G., Law, B. E., Lindroth, A., Merbold, L., Montagnani, L., Moors, E. J., Papale, D., Sottocornola, M., Vaccari, F., and Williams, C.: Global patterns of land-atmosphere fluxes of carbon dioxide, latent heat, and sensible heat derived from eddy covariance, satellite, and meteorological observations, Journal of Geophysical Research: Biogeosciences, 116, n/a–n/a, doi:10.1029/2010JG001566, http://dx.doi.org/10.1029/2010JG001566, g00J07, 2011.

Key, R. M., Kozyr, A., Sabine, C. L., Lee, K., Wanninkhof, R., Bullister, J. L., Feely, R. A., Millero, F. J., Mordy, C., and Peng, T.-H.: A global ocean carbon climatology: Results from Global Data Analysis Project (GLODAP), Global Biogeochemical Cycles, 18, n/a–n/a, doi:10.1029/2004GB002247, http://dx.doi.org/10.1029/2004GB002247, gB4031, 2004.

Knorr, W. and Heimann, M.: Uncertainties in global terrestrial biosphere modeling: 1. A comprehensive sensitivity analysis with a new photosynthesis and energy balance scheme, Global Biogeochemical Cycles, 15, 207–225, doi:10.1029/1998GB001059, http://dx.doi.org/10.1029/1998GB001059, 2001.

Koffi, E. N., Rayner, P. J., Scholze, M., and Beer, C.: Atmospheric constraints on gross primary productivity and net ecosystem productivity: Results from a carbon-cycle data assimilation system, Global Biogeochemical Cycles, 26, n/a–n/a, doi:10.1029/2010GB003900, http://dx.doi.org/10.1029/2010GB003900, gB1024, 2012.

Kowalczyk, E. A., Wang, Y. P., Law, R. M., Davies, H. L., McGregor, J. L., and Abramowitz, G.: The CSIRO Atmosphere Biosphere Land Exchange (CABLE) model for use in climate models and as an offline model, CSIRO Marine and Atmospheric Research technical paper 13, 2006.

Law, R. M., Ziehn, T., Matear, R. J., Lenton, A., Chamberlain, M. A., Stevens, L., Wang, Y.-P., Bi, D., and Yan, H.: The carbon cycle in the Australian Climate and Earth System Simulator (ACCESS-ESM1). 1. Model description and pre-industrial simulation, Geoscientific Model Development, xx, xx–xx, 2015.

Le Quéré, C., Moriarty, R., Andrew, R. M., Peters, G. P., Ciais, P., Friedlingstein, P., Jones, S. D., Sitch, S., Tans, P., Arneth, A., Boden, T. A., Bopp, L., Bozec, Y., Canadell, J. G., Chini, L. P., Chevallier, F., Cosca, C. E., Harris, I., Hoppema, M., Houghton, R. A., House, J. I., Jain, A. K., Johannessen, T., Kato, E., Keeling, R. F., Kitidis, V., Klein Goldewijk, K., Koven, C., Landa, C. S., Landschützer, P., Lenton, A., Lima, I. D., Marland, G., Mathis, J. T., Metzl, N., Nojiri, Y., Olsen, A., Ono, T., Peng, S., Peters, W., Pfeil, B., Poulter, B., Raupach, M. R., Regnier, P., Rödenbeck, C., Saito, S., Salisbury, J. E., Schuster, U., Schwinger, J., Séférian, R., Segschneider, J., Steinhoff, T., Stocker, B. D., Sutton, A. J., Takahashi, T., Tilbrook, B., van der Werf, G. R., Viovy, N., Wang, Y.-P., Wanninkhof, R., Wiltshire, A., and Zeng, N.:

Geosci. Model Dev. Discuss., doi:10.5194/gmd-2016-14, 2016
Manuscript under review for journal Geosci. Model Dev.
Published: 10 May 2016




Global carbon budget 2014, Earth System Science Data, 7, 47–85, doi:10.5194/essd-7-47-2015, http://www.earth-syst-sci-data.net/7/47/2015/, 2015.

Lenton, A., Tilbrook, B., Law, R. M., Bakker, D., Doney, S. C., Gruber, N., Ishii, M., Hoppema, M., Lovenduski, N. S., Matear, R. J., McNeil, B. I., Metzl, N., Mikaloff Fletcher, S. E., Monteiro, P. M. S., Rödenbeck, C., Sweeney, C., and Takahashi, T.: Sea-air $CO_2$ fluxes in the Southern Ocean for the period 1990-2009, Biogeosciences, 10, 4037–4054, doi:10.5194/bg-10-4037-2013, http://www.biogeosciences.net/10/4037/2013/, 2013.

Lenton, A., McInnes, K. L., and O'Grady, J. G.: Marine projections of warming and ocean acidification in the Australasian region, Australian Meteorological and Oceanographic Journal, in press, 2015.

Lewis, S. and Karoly, D.: Assessment of forced responses of the Australian Community Climate and Earth System Simulator (ACCESS) 1.3 in CMIP5 historical detection and attribution experiments, Australian Meteorological and Oceanographic Journal, 64, 87–101, 2014.

Los, S. O., Collatz, G. J., Sellers, P. J., Malmstrsm, C. M., Pollack, N. H., DeFries, R. S., Bounoua, L., Parris, M. T., Tucker, C. J., and Dazlich, D. A.: A global 9-year biophysical land-surface data set from NOAA AVHRR data, J. Hydrometeor., 1, 183–199, 2000.

Martinez, E., Antoine, D., D'Ortenzio, F., and Gentili, B.: Climate-Driven Basin-Scale Decadal Oscillations of Oceanic Phytoplankton, Science, 326, 1253–1256, doi:10.1126/science.1177012, http://www.sciencemag.org/content/326/5957/1253.abstract, 2009.

Oke, P. R., Griffin, D. A., Schiller, A., Matear, R. J., Fiedler, R., Mansbridge, J., Lenton, A., Cahill, M., Chamberlain, M. A., and Ridgeway, K.: Evaluation of a near-global eddy-resolving ocean model, Geosci. Model Dev., 6, 591–615, doi:10.5194/gmd-6-591-2013, 2013.

Piao, S., Ciais, P., Friedlingstein, P., de Noblet-Ducoudré, N., Cadule, P., Viovy, N., and Wang, T.: Spatiotemporal patterns of terrestrial carbon cycle during the 20th century, Global Biogeochemical Cycles, 23, n/a–n/a, doi:10.1029/2008GB003339, http://dx.doi.org/10.1029/2008GB003339, gB4026, 2009.

Post, W., Pastor, J., Zinke, P. J., and Stangenberger, A. G.: Global patterns of soil nitrogen storage, Nature, 317, 613–616, 1985.

Prentice, I. C., Farquhar, G. D., Fasham, M. J. R., Goulden, M. L., Heimann, M., Jaramillo, V. J., Kheshgi, H. S., Quéré, C. L., Scholes, R. J., and Wallace, D.: The carbon cycle and atmospheric carbon dioxide, in: Climate Change 2001: The Scientific Basis. Contri- bution of Working Group I to the Third Assessment Report of the Intergovernmental Panel on Climate Change, edited by Houghton, J. T., Ding, Y., Griggs, D. J., Noguer, M., van der Linden, P. J., Dai, X., Maskell, K., and Johnson, C., Cambridge University Press, Cambridge, UK and New York, NY, 2001.

Rayner, N. A., Parker, D. E., Horton, E. B., Folland, C. K., Alexander, L. V., Rowell, D. P., Kent, E. C., and Kaplan, A.: Global analyses of sea surface temperature, sea ice, and night marine air temperature since the late nineteenth century, Journal of Geophysical Research: Atmospheres, 108, n/a–n/a, doi:10.1029/2002JD002670, http://dx.doi.org/10.1029/2002JD002670, 4407, 2003.

Rotstayn, L. D., Collier, M. A., and Luo, J.-J.: Effects of declining aerosols on projections of zonally averaged tropical precipitation, Environmental Research Letters, 10, 044 018, http://stacks.iop.org/1748-9326/10/i=4/a=044018, 2015.

Sabine, C. L., Feely, R. A., Gruber, N., Key, R. M., Lee, K., Bullister, J. L., Wanninkhof, R., Wong, C. S., Wallace, D. W. R., Tilbrook, B., Millero, F. J., Peng, T.-H., Kozyr, A., Ono, T., and Rios, A. F.: The Oceanic Sink for Anthropogenic CO2, Science, 305, 367–371, doi:10.1126/science.1097403, http://www.sciencemag.org/content/305/5682/367.abstract, 2004.

Sallée, J.-B., Shuckburgh, E., Bruneau, N., Meijers, A. J. S., Bracegirdle, T. J., and Wang, Z.: Assessment of Southern Ocean mixed-layer depths in CMIP5 models: Historical bias and forcing response, Journal of Geophysical Research: Oceans, 118, 1845–1862, doi:10.1002/jgrc.20157, http://dx.doi.org/10.1002/jgrc.20157, 2013.

Sato, M., Hansen, J., Lacis, A., and Thomason, L.: Stratospheric Aerosol Optical Thickness, http://data.giss.nasa.gov/modelforce/strataer/, 2002.



Scharlemann, J. P., Tanner, E. V., Hiederer, R., and Kapos, V.: Global soil carbon: understanding and managing the largest terrestrial carbon pool, Carbon Management, 5, 81–91, doi:10.4155/cmt.13.77, http://dx.doi.org/10.4155/cmt.13.77, 2014.

Schlesinger, W.: Biogeochemistry: An Analysis of Global Change, Academic Press, 1997.

Shao, P., Zeng, X., Sakaguchi, K., Monson, R. K., and Zeng, X.: Terrestrial Carbon Cycle: Climate Relations in Eight CMIP5 Earth System Models, J. Climate, 26, 8744–8764, 2013.

Smil, V.: PHOSPHORUS IN THE ENVIRONMENT: Natural Flows and Human Interferences, Annual Review of Energy and the Environment, 25, 53–88, doi:10.1146/annurev.energy.25.1.53, http://dx.doi.org/10.1146/annurev.energy.25.1.53, 2000.

Stenchikov, G., Delworth, T. L., Ramaswamy, V., Stouffer, R. J., Wittenberg, A., and Zeng, F.: Volcanic signals in oceans, Journal of Geophysical Research: Atmospheres, 114, n/a–n/a, doi:10.1029/2008JD011673, http://dx.doi.org/10.1029/2008JD011673, d16104, 2009.

Stott, P. A., Jones, G. S., Lowe, J. A., Thorne, P., Durman, C., Johns, T. C., , and Thelen, J.-C.: Transient climate simulations with the hadgem1 climate model: causes of past warming and future climate change., J. Climate, 19, 2763–2782, http://dx.doi.org/10.1175/JCLI3731.1, 2006.

Takahashi, T., Sutherland, S. C., Wanninkhof, R., Sweeney, C., Feely, R. A., Chipman, D. W., Hales, B., Friederich, G., Chavez, F., Sabine, C., Watson, A., Bakker, D. C., Schuster, U., Metzl, N., Yoshikawa-Inoue, H., Ishii, M., Midorikawa, T., Nojiri, Y., Körtzinger, A., Steinhoff, T., Hoppema, M., Olafsson, J., Arnarson, T. S., Tilbrook, B., Johannessen, T., Olsen, A., Bellerby, R., Wong, C., Delille, B., Bates, N., and de Baar, H. J.: Climatological mean and decadal change in surface ocean pCO2, and net sea–air {CO2} flux over the global oceans, Deep Sea Research Part II: Topical Studies in Oceanography, 56, 554 – 577, doi:http://dx.doi.org/10.1016/j.dsr2.2008.12.009, http://www.sciencedirect.com/science/article/pii/S0967064508004311, surface Ocean {CO2} Variability and Vulnerabilities, 2009.

Taylor, K. E., Stouffer, R. J., and Meehl, G. A.: An Overview of CMIP5 and the experiment design, Bull. Amer. Meteor. Soc., 93, 485–498, doi:10.1175/BAMS-D-11-00094.1., 2012.

Todd-Brown, K. E. O., Randerson, J. T., Post, W. M., Hoffman, F. M., Tarnocai, C., Schuur, E. A. G., and Allison, S. D.: Causes of variation in soil carbon simulations from CMIP5 Earth system models and comparison with observations, Biogeosciences, 10, 1717–1736, doi:10.5194/bg-10-1717-2013, http://www.biogeosciences.net/10/1717/2013/, 2013.

Wang, Y.-P. and Houlton, B. Z.: Nitrogen constraints on terrestrial carbon uptake: Implications for the global carbon-climate feedback, Geophysical Research Letters, 36, n/a–n/a, doi:10.1029/2009GL041009, http://dx.doi.org/10.1029/2009GL041009, l24403, 2009.

Wang, Y. P., Law, R. M., and Pak, B.: A global model of carbon, nitrogen and phosphorus cycles for the terrestrial biosphere, Biogeosciences, 7, 2261–2282, doi:10.5194/bg-7-2261-2010, 2010.

Wang, Y. P., Kowalczyk, E., Leuning, R., Abramowitz, G., Raupach, M. R., Pak, B., van Gorsel, E., and Luhar, A.: Diagnosing errors in a land surface model (CABLE) in the time and frequency domains, J. Geophys. Res., 116, G01 034, doi:10.1029/2010JG001385, 2011.

Wanninkhof, R., Park, G. H., Takahashi, T., Sweeney, C., Feely, R., Nojiri, Y., Gruber, N., Doney, S. C., McKinley, G. A., Lenton, A., Le Quéré, C., Heinze, C., Schwinger, J., Graven, H., and Khatiwala, S.: Global ocean carbon uptake: magnitude, variability and trends, Biogeosciences, 10, 1983–2000, doi:10.5194/bg-10-1983-2013, http://www.biogeosciences.net/10/1983/2013/, 2013.

Welp, L., Keeling, R., Meijer, H., Bollenbacher, A., Piper, S., Yoshimura, K., Francey, R., Allison, C., and Wahlen, M.: Interannual variability in the oxygen isotopes of atmospheric CO2 driven by El Nino, Nature, 477, 579–582, doi:10.1038/nature10421, 2011.

Wieder, W. R., Boehnert, J., and Bonan, G. B.: Evaluating soil biogeochemistry parameterizations in Earth system models with observations, Global Biogeochemical Cycles, 28, 211–222, doi:10.1002/2013GB004665, http://dx.doi.org/10.1002/2013GB004665, 2014.



Yang, W., Tan, B., Huang, D., Rautiainen, M., Shabanov, N., Wang, Y., Privette, J., Huemmrich, K., Fensholt, R., Sandholt, I., Weiss, M., Ahl, D., Gower, S., Nemani, R., Knyazikhin, Y., and Myneni, R.: MODIS leaf area index products: from validation to algorithm improvement, Geoscience and Remote Sensing, IEEE Transactions on, 44, 1885–1898, doi:10.1109/TGRS.2006.871215, 2006.

Zeng, N., Mariotti, A., and Wetzel, P.: Terrestrial mechanisms of interannual CO2 variability, Global Biogeochemical Cycles, 19, n/a–n/a, doi:10.1029/2004GB002273, http://dx.doi.org/10.1029/2004GB002273, gB1016, 2005.

Zhang, Q., Pitman, A. J., Wang, Y. P., Dai, Y. J., and Lawrence, P. J.: The impact of nitrogen and phosphorous limitation on the estimated terrestrial carbon balance and warming of land use change over the last 156 yr, Earth Syst. Dynam., 4, 333–345, doi:10.5194/esd-4-333-2013, 2013.

Zhu, Z., Bi, J., Pan, Y., Ganguly, S., Anav, A., Xu, L., Samanta, A., Piao, S., Nemani, R. R., and Myneni, R. B.: Global Data Sets of Vegetation Leaf Area Index (LAI)3g and Fraction of Photosynthetically Active Radiation (FPAR)3g Derived from Global Inventory Modeling and Mapping Studies (GIMMS) Normalized Difference Vegetation Index (NDVI3g) for the Period 1981 to 2011, Remote Sensing, 5, 927, doi:10.3390/rs5020927, http://www.mdpi.com/2072-4292/5/2/927, 2013.

Ziehn, T., Kattge, J., Knorr, W., and Scholze, M.: Improving the predictability of global CO2 assimilation rates under climate change, Geophysical Research Letters, 38, n/a–n/a, doi:10.1029/2011GL047182, http://dx.doi.org/10.1029/2011GL047182, l10404, 2011.

Geosci. Model Dev. Discuss., doi:10.5194/gmd-2016-14, 2016
Manuscript under review for journal Geosci. Model Dev.
Published: 10 May 2016


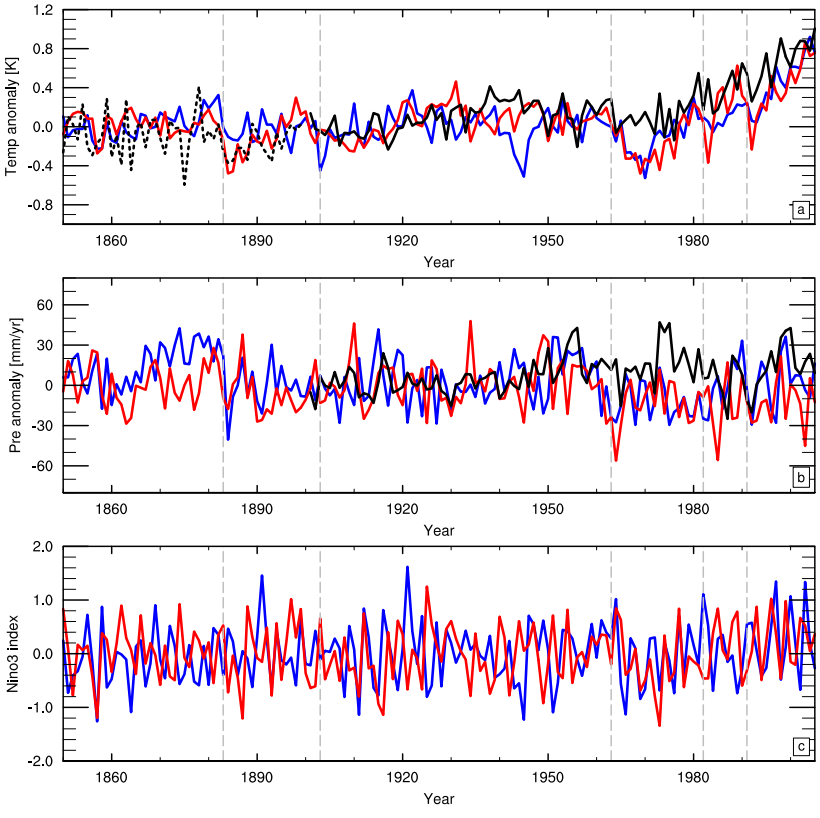


**Figure 1.** Anomalies (reference period: 1901-1930) for **(a)** globally averaged surface air temperature and **(b)** globally averaged precipitation for land points only for ACCESS-ESM1 (PresLAI, blue; ProgLAI, red) and observed CRU (black, dashed before 1901). Major volcanic eruptions are marked with dashed lines: Krakatoa (1983), Santa Maria (1903), Mt. Agung (1963), El Chichón (1982) and Mt. Pinatubo (1991).

Geosci. Model Dev. Discuss., doi:10.5194/gmd-2016-14, 2016
Manuscript under review for journal Geosci. Model Dev.
Published: 10 May 2016


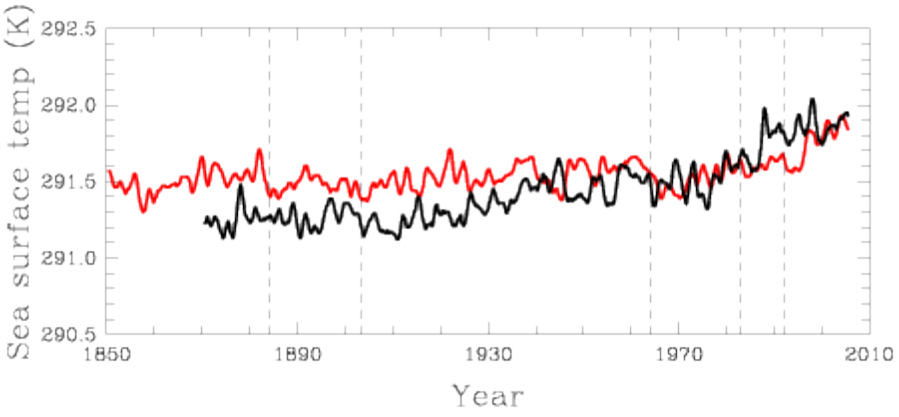


**Figure 2.** Globally averaged sea surface temperature (K) between 1850- 2005, red is ACCESS-ESM1 and black is HadiSST (Rayner et al., 2003). Major volcanic eruptions are marked with dashed lines: Krakatoa (1983), Santa Maria (1903), Mt. Agung (1963), El Chichón (1982) and Mt. Pinatubo (1991).

Geosci. Model Dev. Discuss., doi:10.5194/gmd-2016-14, 2016
Manuscript under review for journal Geosci. Model Dev.
Published: 10 May 2016


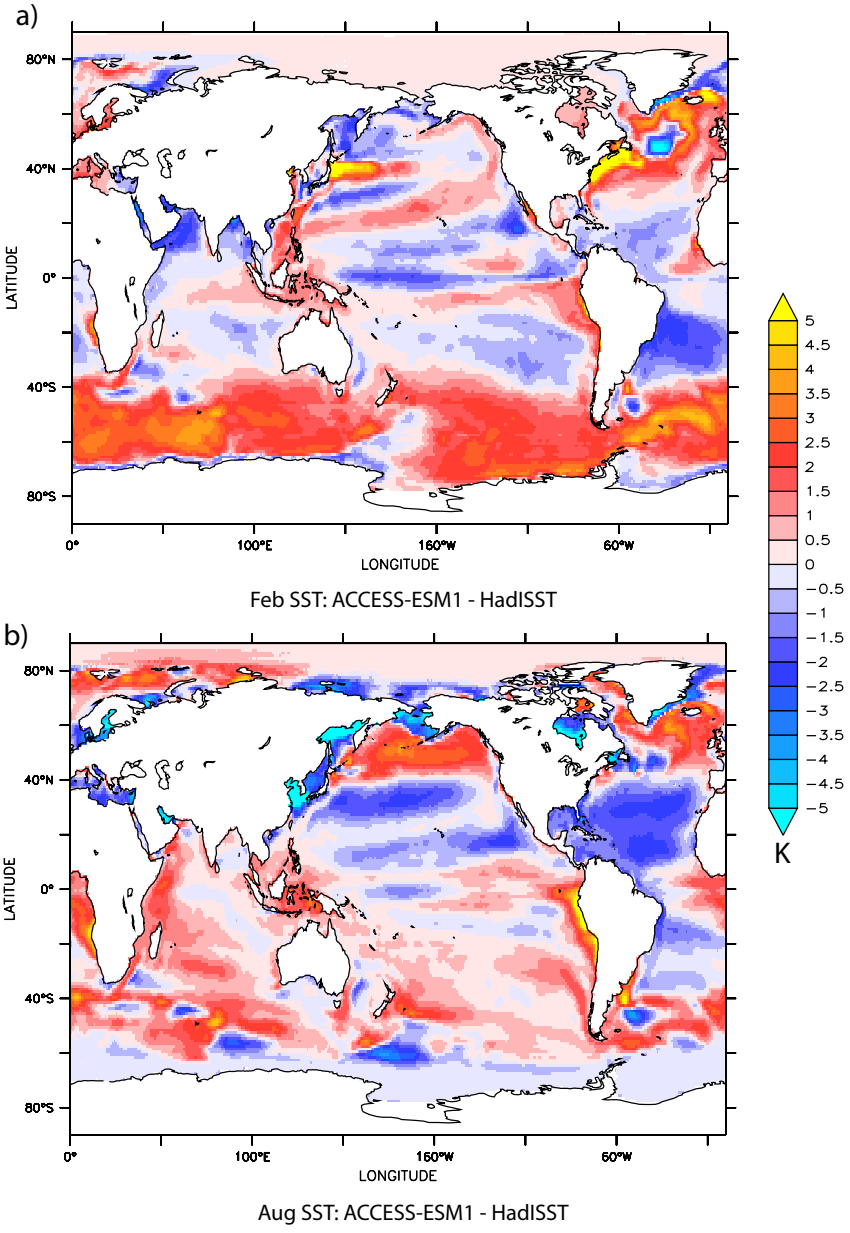


**Figure 3.** Differences in sea surface temperature (K) between ACCESS-ESM1 and HadiSST for **(a)** February and **(b)** August.

Geosci. Model Dev. Discuss., doi:10.5194/gmd-2016-14, 2016
Manuscript under review for journal Geosci. Model Dev.
Published: 10 May 2016


Geoscientific Model Development Discussions
Open Access
EGU

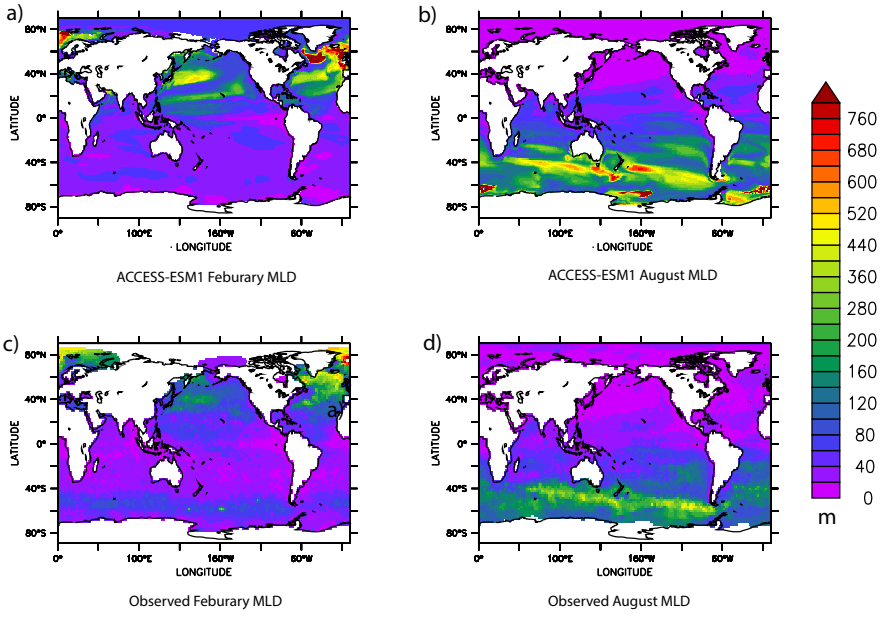


**Figure 4.** Differences in mixed layer depth between ACCESS-ESM1 and observations from de Boyer Montégut et al. (2004). The mixed layer is calculated based on a 0.03 kg/m$^3$ density change from the surface ocean. Differences are shown for **(a,c)** February and for **(b,d)** August.

Geosci. Model Dev. Discuss., doi:10.5194/gmd-2016-14, 2016
Manuscript under review for journal Geosci. Model Dev.
Published: 10 May 2016


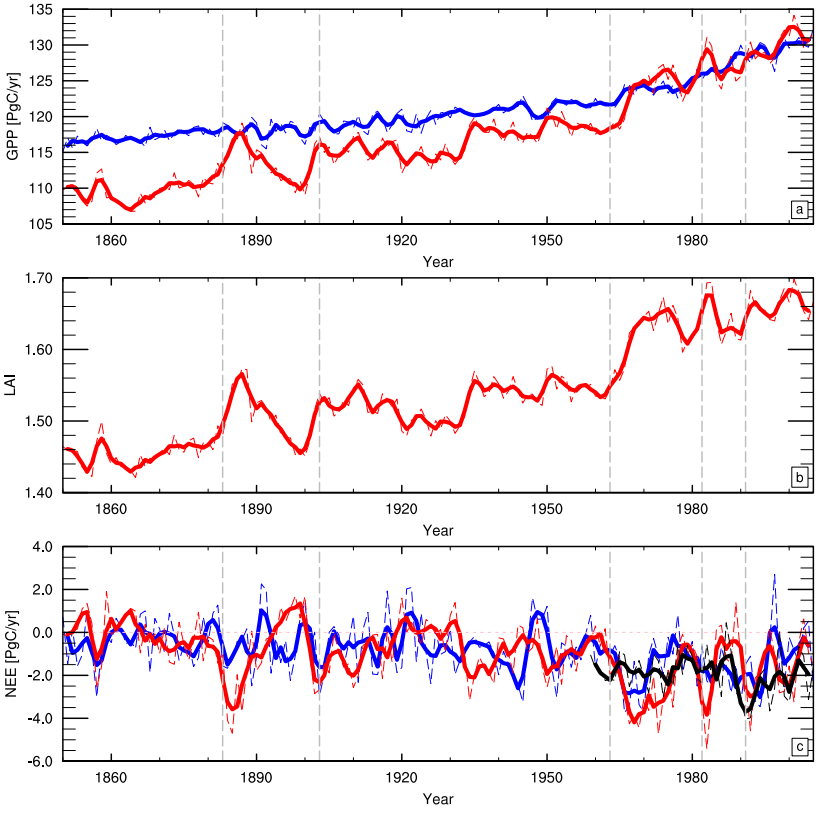


**Figure 5.** Temporal evolution of **(a)** GPP ($\mathrm{PgC\,yr^{-1}}$), **(b)** LAI and **(c)** NEE ($\mathrm{PgC\,yr^{-1}}$). GCP estimates for NEE are shown for comparison in black for the years 1959-2005. ACCESS-ESM1 results are shown for PresLAI (blue line) and ProgLAI (red line) with annual values marked in thin dashed lines and a 5 yr running mean in heavy solid lines. Major volcanic eruptions are marked with dashed lines: Krakatoa (1983), Santa Maria (1903), Mt. Agung (1963), El Chichón (1982) and Mt. Pinatubo (1991).

Geosci. Model Dev. Discuss., doi:10.5194/gmd-2016-14, 2016
Manuscript under review for journal Geosci. Model Dev.
Published: 10 May 2016


Geoscientific Model Development Discussions

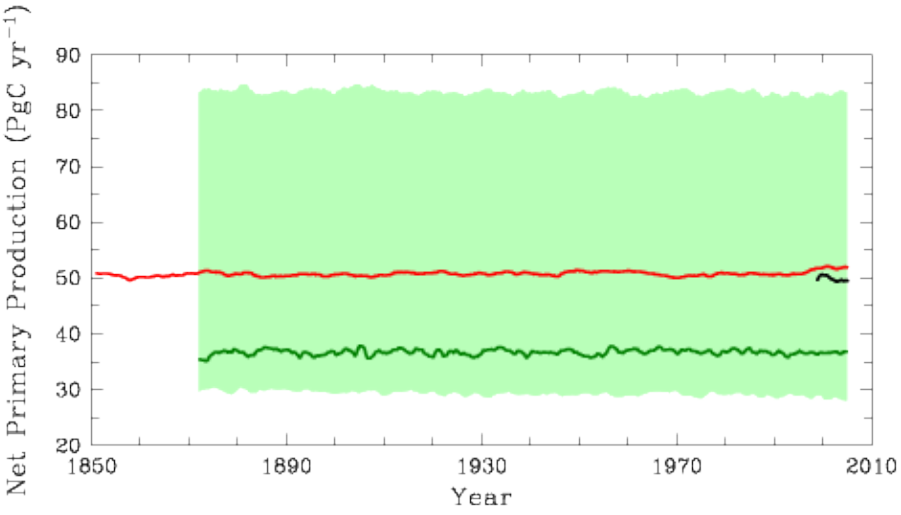


**Figure 6.** Comparison of Integrated Primary Production ($\mathrm{PgC\,yr^{-1}}$) in the period 1850-2005 between CMIP5 and ACCESS-ESM1. The solid red line represents the integrated carbon uptake in $\mathrm{PgC\,yr^{-1}}$ from ACCESS-ESM1, while the green line represents the median of the CMIP5, model with the range overlain (as shaded area) as the 10th and 90th percentiles. Overlain on this plot are the observed values from SeaWIFS over the period 1998-2005 in black.

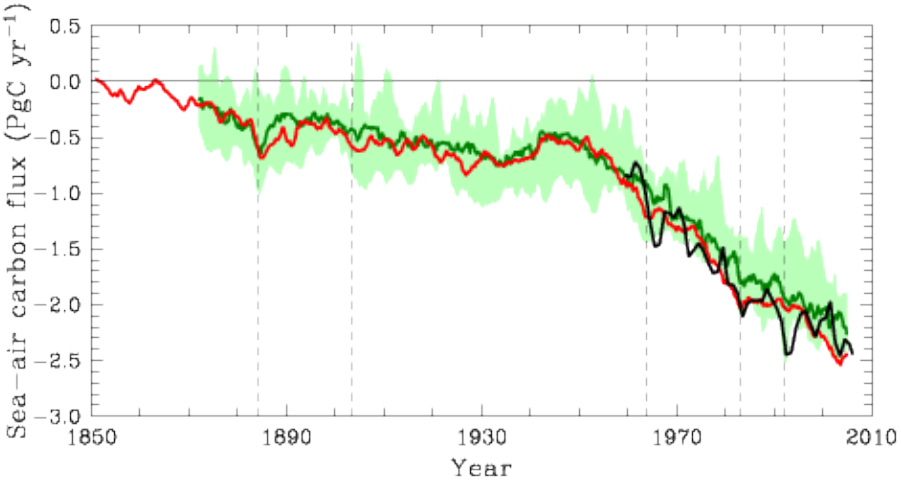


**Figure 7.** Comparison of sea-air $CO_2$ fluxes ($\mathrm{PgC\,yr^{-1}}$) in the period 1850-2005 carbon uptake from ACCESS-ESM1. The solid green line represents the median of the CMIP5, while the shaded are represents the 10th and 90th percentiles of the CMIP5 model. Overlain on this is the estimated sea-air fluxes from the Global Carbon Project (Le Quéré et al., 2015) in black; and the timing of major volcano eruptions over the historical period.

Geosci. Model Dev. Discuss., doi:10.5194/gmd-2016-14, 2016
Manuscript under review for journal Geosci. Model Dev.
Published: 10 May 2016


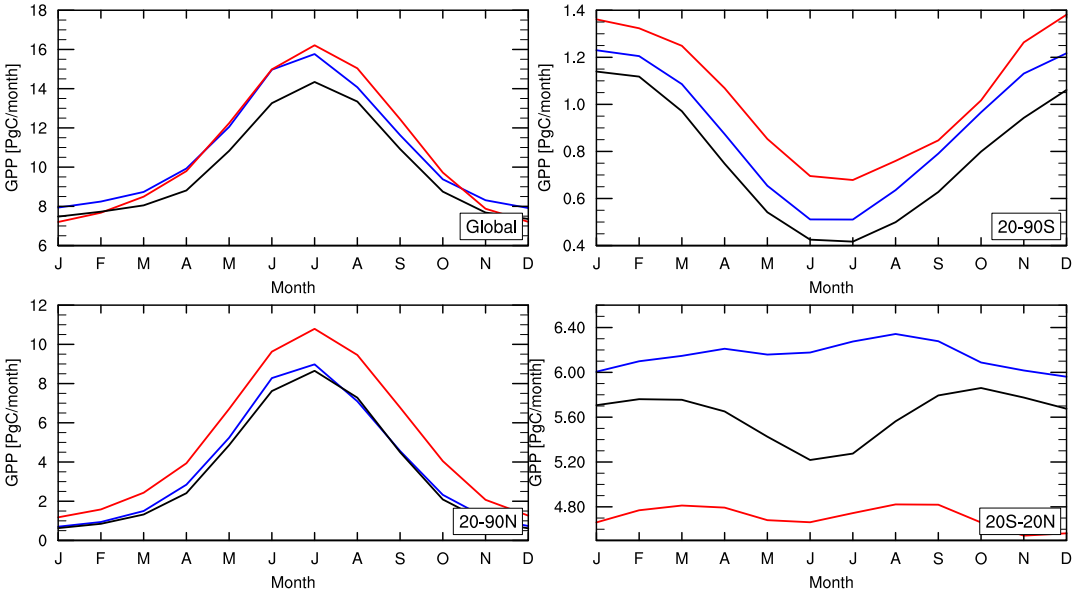


**Figure 8.** Mean annual cycle of GPP ($\mathrm{PgC\,month^{-1}}$) for the period 1986-2005. ACCESS-ESM1 results are shown in blue (PresLAI) and red (ProgLAI). Observation based estimates are shown in black.

Geosci. Model Dev. Discuss., doi:10.5194/gmd-2016-14, 2016
Manuscript under review for journal Geosci. Model Dev.
Published: 10 May 2016


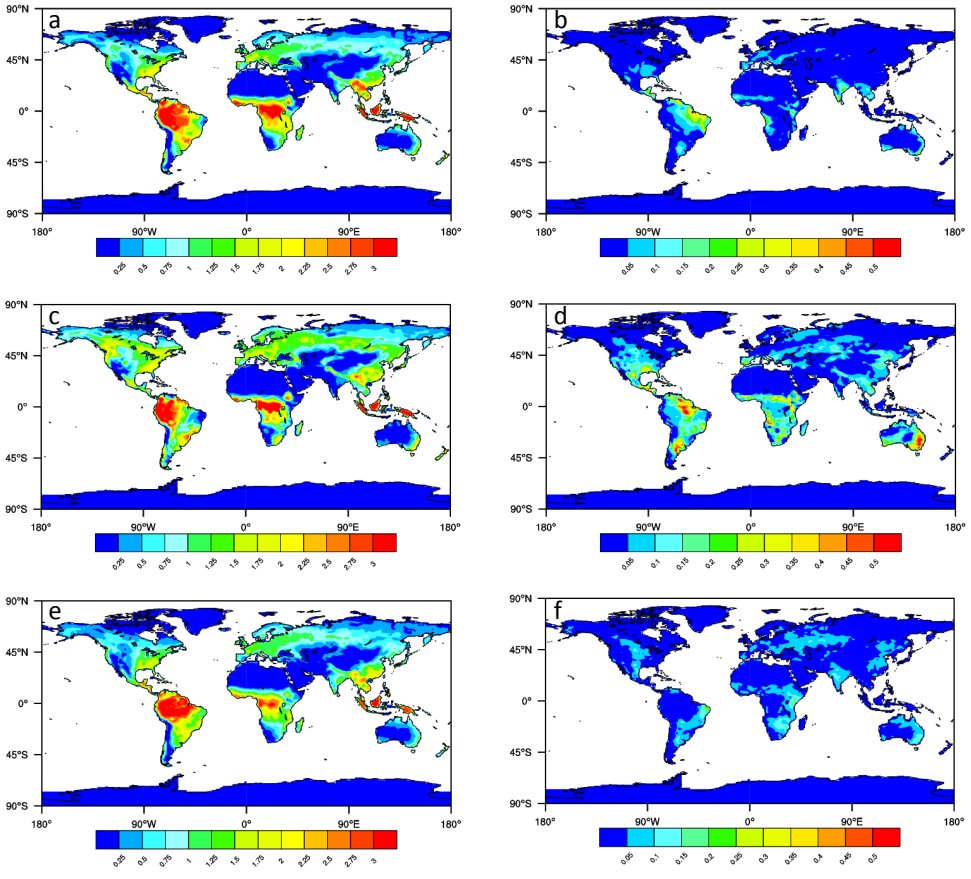


**Figure 9.** Spatial distribution of **(a,c,e)** GPP and **(b,d,f)** GPP IAV ($\mathrm{kgC\,m^{-2}\,yr^{-1}}$) for **(a,b)** PresLAI, **(c,d)** ProgLAI and **(e,f)** observation based estimates.

Geosci. Model Dev. Discuss., doi:10.5194/gmd-2016-14, 2016
Manuscript under review for journal Geosci. Model Dev.
Published: 10 May 2016


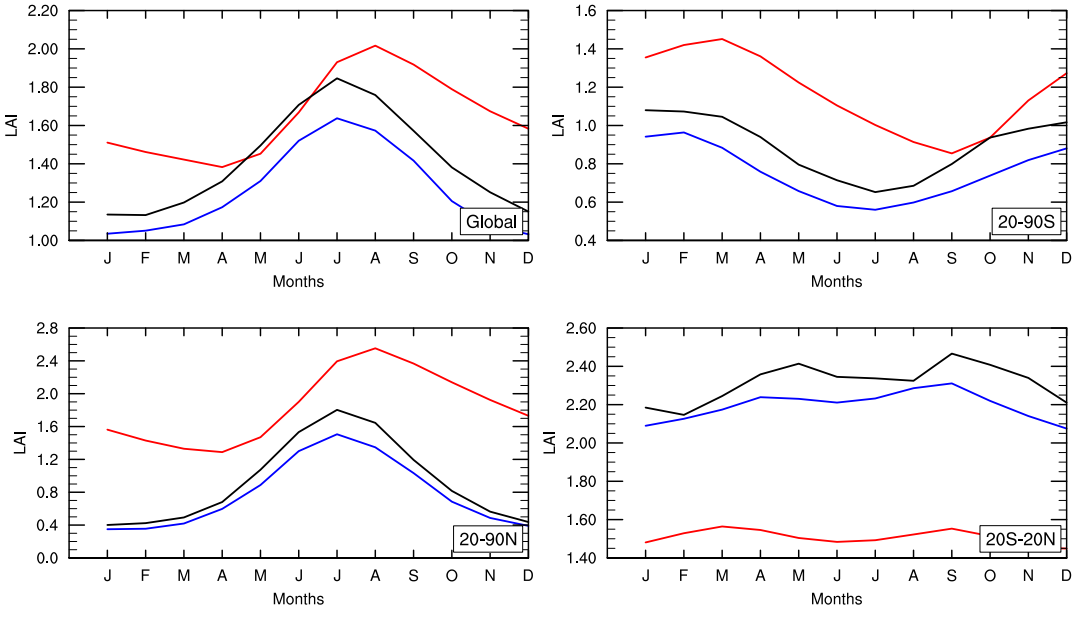


**Figure 10.** Mean annual cycle of LAI for the period 1986-2005. ACCESS-ESM1 results are shown in blue (scenario with prescribed LAI) and red (scenario with prognostic LAI). Observation based estimates are shown in black.

Geosci. Model Dev. Discuss., doi:10.5194/gmd-2016-14, 2016
Manuscript under review for journal Geosci. Model Dev.
Published: 10 May 2016


Geoscientific Model Development Discussions
Open Access
EGU

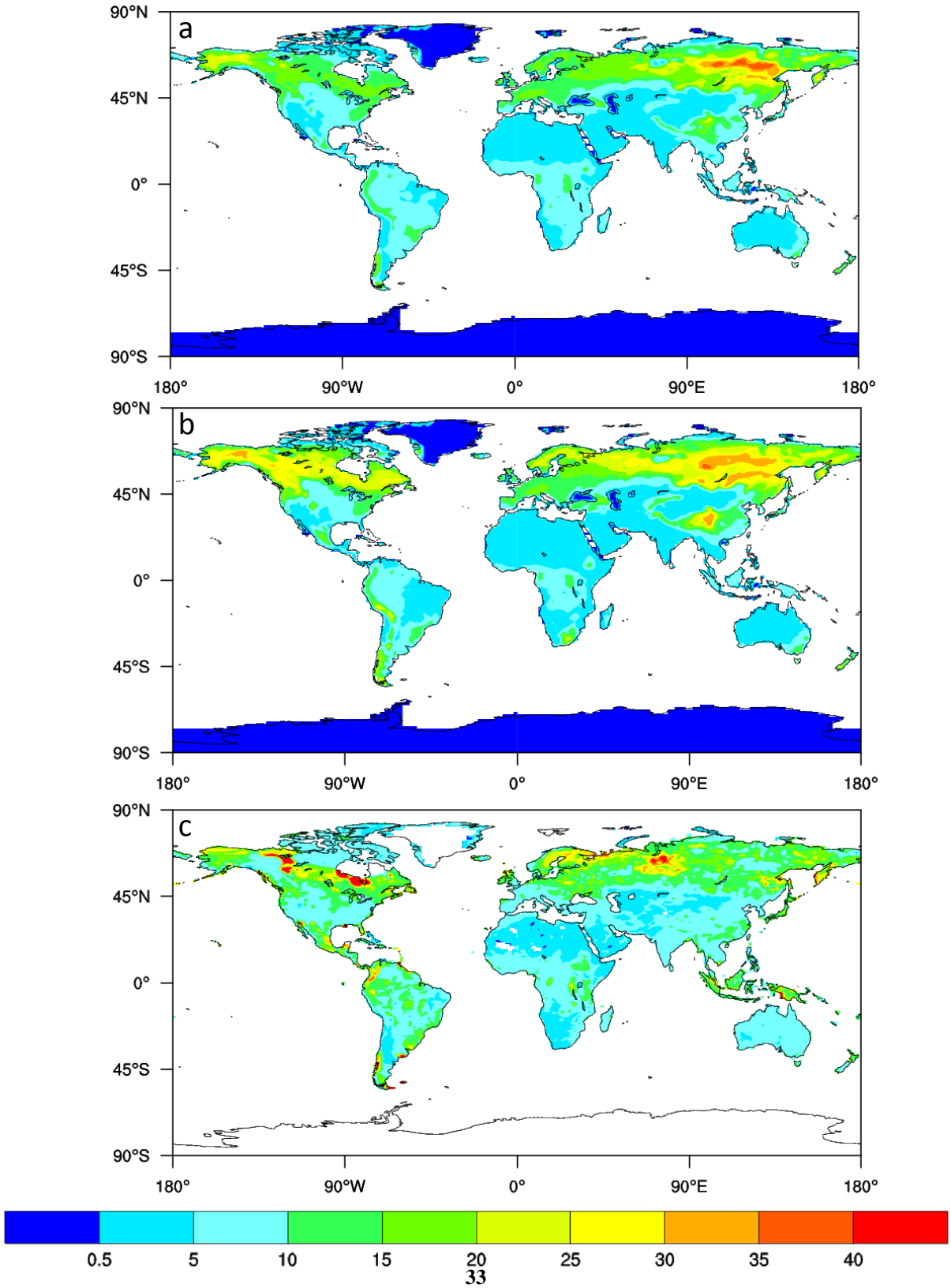




**Figure 11.** Spatial distribution of organic soil carbon ($kgC\,m^{-2}$) (a) using prescribed LAI, (b) using prognostic LAI and (c) observation based estimated from HWSD.

Geosci. Model Dev. Discuss., doi:10.5194/gmd-2016-14, 2016
Manuscript under review for journal Geosci. Model Dev.
Published: 10 May 2016


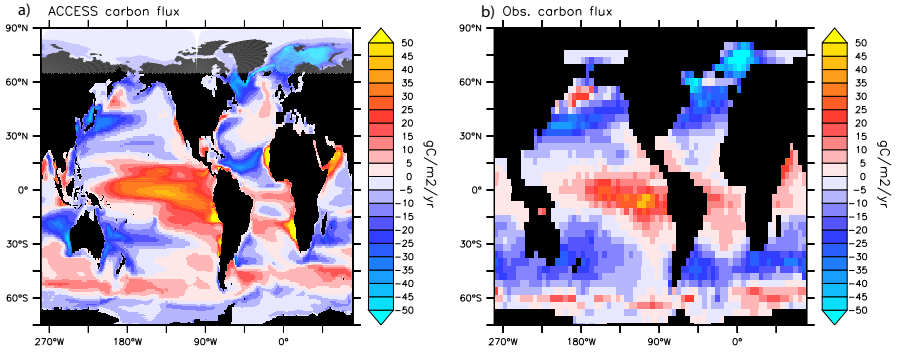


**Figure 12.** The integrated sea-air $CO_2$ fluxes over the period 1986-2005 from **(a)** ACCESS-ESM1 and **(b)** Wanninkhof et al. (2013)

Geosci. Model Dev. Discuss., doi:10.5194/gmd-2016-14, 2016
Manuscript under review for journal Geosci. Model Dev.
Published: 10 May 2016


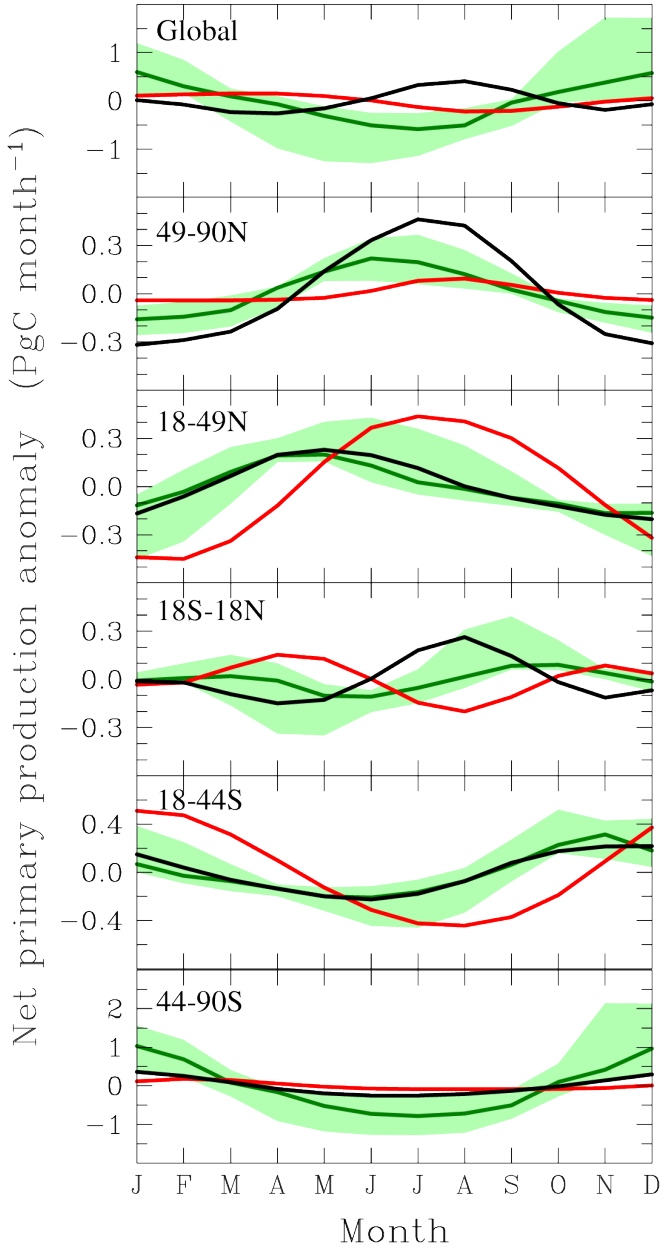


**Figure 13.** The seasonal cycle of integrated net primary production anomalies (PgC month$^{-1}$) from ACCESS-ESM1 in red and SeaWIFS (Behrenfeld and Falkowski, 1997) in black. Overlain on this plot is the CMIP5 the median (solid green line) and the range 10th and 90th percentiles (shaded) over the period 1998-2005.

Geosci. Model Dev. Discuss., doi:10.5194/gmd-2016-14, 2016
Manuscript under review for journal Geosci. Model Dev.
Published: 10 May 2016


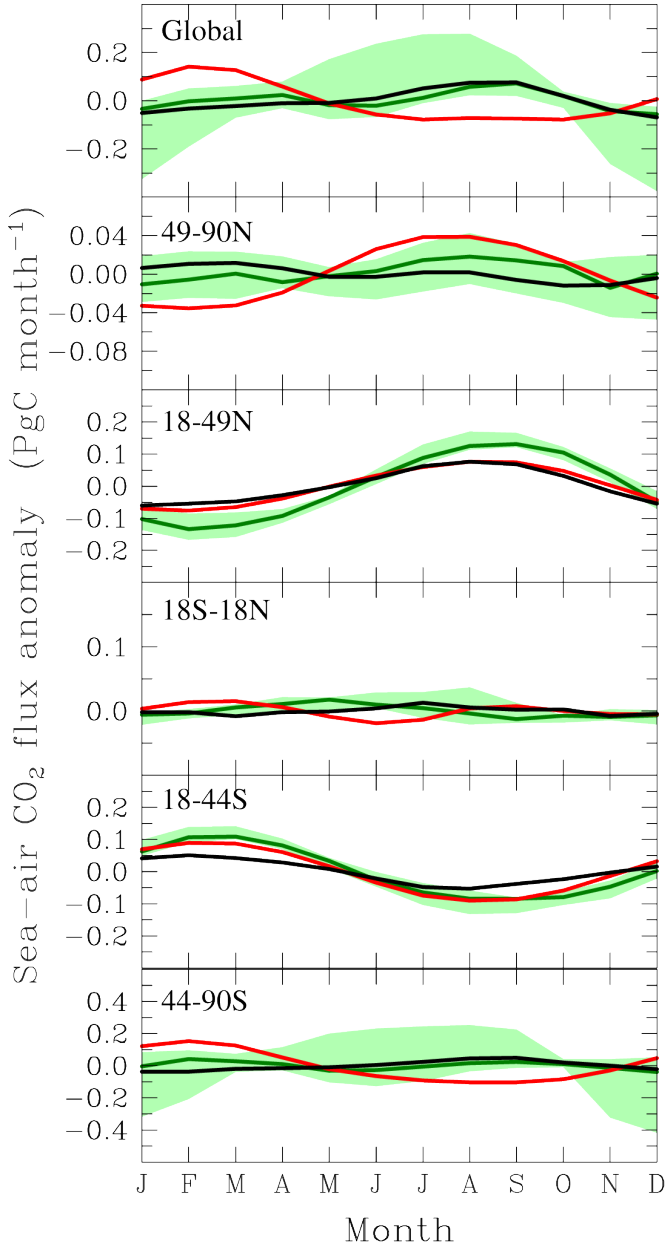


**Figure 14.** The seasonal cycle (1986-2005) of sea-air $CO_2$ flux anomalies ($\mathrm{PgC\,month^{-1}}$) from ACCESS-ESM1 (red line) and observations ((Wanninkhof et al., 2013); black line). Overlain is the CMIP5 median (solid green line) and the range as the 10th and 90th percentiles (shaded).

Geosci. Model Dev. Discuss., doi:10.5194/gmd-2016-14, 2016
Manuscript under review for journal Geosci. Model Dev.
Published: 10 May 2016


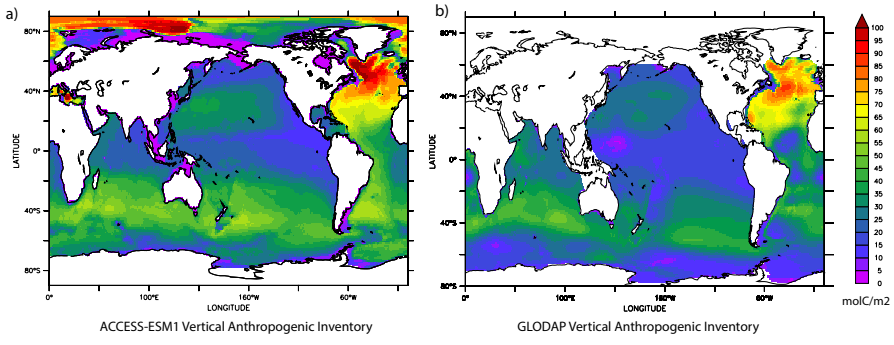


**Figure 15.** Column inventory of Anthropogenic Carbon in the ocean (molC/m2) from **(a)** ACCESS-ESM1 and from **(b)** GLODAP (Sabine et al. (2004); Key et al. (2004) for 1994.

Geosci. Model Dev. Discuss., doi:10.5194/gmd-2016-14, 2016
Manuscript under review for journal Geosci. Model Dev.
Published: 10 May 2016


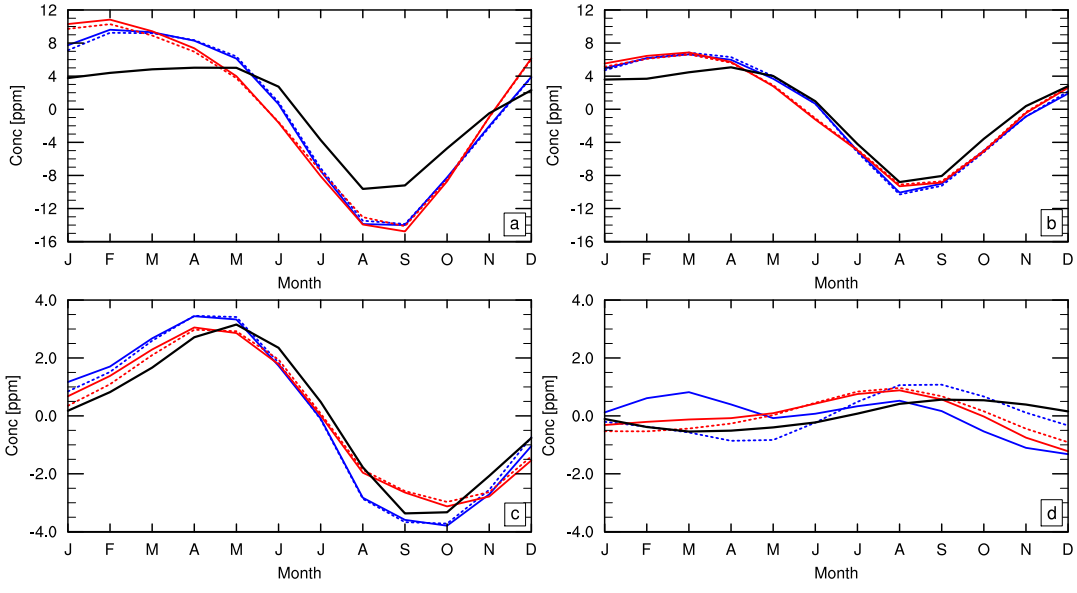


**Figure 16.** Mean seasonal cycle of atmospheric $CO_2$ for the period 1986-2005 from land carbon fluxes (dashed lines) and both land and ocean carbon fluxes (solid line). The prescribed LAI case is shown in blue, the prognostic LAI case in red and observations based on flask data from GLOBALVIEW in black for **(a)** Alert (82.45° N, 62.52° W), **(b)** Mace Head (53.33° N, 9.90° W), **(c)** Mauna Loa (19.53° N, 155.58° W) and **(d)** South Pole (89.98° S, 24.80° W).

Geosci. Model Dev. Discuss., doi:10.5194/gmd-2016-14, 2016
Manuscript under review for journal Geosci. Model Dev.
Published: 10 May 2016


Geoscientific Model Development Discussions
Open Access
EGU

**Table 1.** The CMIP5 models used to assess the ocean response of ACCESS-ESM1 over the historical period in the study. Reference for all models are provided in Lenton et al. (2015).

| Model Name | Institute ID | Modelling Group |
|---|---|---|
| CanESM2 | CCCMA | Canadian Centre for Climate Modelling and Analysis |
| HadGEM-ES | MOHC | Met Office Hadley Centre (additional HadGEM2-ES |
| | (additional realizations by INPE) | realizations contributed by Instituto Nacional de Pesquisas Espaciais) |
| GFDL-ESM2M | NOAA GFDL | NOAA Geophysical Fluid Dynamics Laboratory |
| ISPL-CM5A-LR | IPSL | Institut Pierre-Simon Laplace |
| IPSL-CM5A-MR | IPSL | Institut Pierre-Simon Laplace |
| MPI-ESM-MR | MPI-M | Max-Planck-Institut für Meteorologie |
| | | (Max Planck Institute for Meteorology) |

**Table 2.** Mean carbon (C), Nitrogen (N) and phosphorus (P) pools sizes in Pg for the period 1986-2005. Biomass comprises leaf, wood and root pool.

| | Prescribed LAI | | | Prognostic LAI | | |
|---|---|---|---|---|---|---|
| Pool | C | N | P | C | N | P |
| Biomass | 670 | 6.2 | 0.34 | 807 | 6.84 | 0.37 |
| Litter | 126 | 0.9 | 0.05 | 163 | 1.1 | 0.06 |
| SOC | 1050 | 83.4 | 10.14 | 1217 | 88.53 | 12.59 |